SpeciesBySpecies Pattern Analysis of Coastal Dune Vegetation

Original

SpeciesBySpecies Pattern Analysis of Coastal Dune Vegetation / Demichele, D.; Belcore, E.; Piras, M.; Camporeale, C.. - In: JOURNAL OF GEOPHYSICAL RESEARCH. BIOGEOSCIENCES. - ISSN 2169-8953. - ELETTRONICO. - 130:2(2025). [10.1029/2024jg008419]

Publisher:
John Wiley & Sons

Published
DOI:10.1029/2024jg008419

JGR Biogeosciences

RESEARCH ARTICLE
10.1029/2024JG008419

Special Collection:
Surface Topography and Vegetation: Science, Measurements, and Technologies

Key Points:

- Dune-building plant, controlling the growth of coastal dunes, are also the most susceptible to anthropic disturbances
- Under undisturbed conditions, vegetation threshold distance from the coastline is well-represented by the reaching distance of extreme-events wave runup
- Topography is the main feature controlling spatial patterns on coastal dunes

Supporting Information:

Supporting Information may be found in the online version of this article.

Correspondence to:
D. Demichele,
davide.demichele@polito.it

Citation:
Demichele, D., Belcore, E., Piras, M., & Camporeale, C. (2025). Species-by-species pattern analysis of coastal dune vegetation. *Journal of Geophysical Research: Biogeosciences*, *130*, e2024JG008419. https://doi.org/10.1029/2024JG008419

Received 14 AUG 2024
Accepted 27 JAN 2025

Author Contributions:
Conceptualization: M. Piras, C. Camporeale
Data curation: D. Demichele, E. Belcore
Formal analysis: D. Demichele
Investigation: C. Camporeale
Methodology: D. Demichele, E. Belcore, C. Camporeale
Project administration: C. Camporeale
Resources: E. Belcore
Software: D. Demichele

Species-By-Species Pattern Analysis of Coastal Dune Vegetation

D. Demichele[1], **E. Belcore**[1], **M. Piras**[1], **and C. Camporeale**[1]

[1]DIATI, Department of Environment, Land and Infrastructure Engineering, Politechnic of Turin, Turin, Italy

Abstract Vegetation is crucial for stabilizing and developing coastal dunes. Different plant species exhibit different spatial distributions which reflect their environmental role and adaptation strategy. This study aims to provide a fine-scale species-by-species analysis of vegetation spatial patterns on coastal dunes within the San Rossore–Migliarino–Massacciuccoli Regional Park (Tuscany, Italy). A comprehensive vegetation data set generated by an Object-Based Image Analysis (OBIA) algorithm applied to high-resolution ortho-images has been utilized. A Digital Terrain Model (DTM) of the study area was created to assess the impact of dune morphology on plant distribution. Moreover, a wave runup analysis was also conducted to understand the interaction between vegetation and hydrodynamic forces. The research highlights how the vegetation threshold distance from the coastline, L_{veg}, is superimposed by the reaching distance of wave runup during extreme events. Terrain morphology significantly affects the vegetation zonation: on taller and undisturbed dunefields, species zonation is clearer and more defined, whereas, on flatter and disturbed ones, spatial distribution is significantly fuzzier. A positive correlation emerges between the abundance of a species and its degree of spatial clustering, indicating how less abundant species form more tightly clustered spatial patterns. Modified Ripley's L-function analysis revealed a multi-scale clustered pattern for most species under examination. The present results may provide a solid benchmark in coastal ecology research for supporting natural-based conservation plans and eco-morphodynamic modeling.

Plain Language Summary Vegetation is essential for stabilizing and developing coastal dunes, with different plant species showing unique patterns based on their roles and adaptations. This study analyzes these patterns in a protected zone of the Regional Park in Tuscany, Italy, using high-resolution images and statistical methods. Main findings show how the vegetation threshold distance from the coastline matches wave runup during extreme events. Dune size is linked to the abundance of the dune-building species like *Ammophila arenaria*, while dune shape heavily affects vegetation spatial arrangement. The abundance of a plant species affects its spatial density and clustering level, with less abundant species showing more variability and tighter clustering. Knowledge advancement brought by this study may provide support as a benchmark study for natural-based solutions for coastal conservation.

1. Introduction

Coastal dunes stand as vital ecosystems that play a pivotal role in maintaining coastal resilience and supporting diverse forms of life (J. Clark, 1977; Hesp, 1991; Martínez & Psuty, 2004). As nature's protective barrier between land and sea, coastal dunes preserve biodiversity, mitigate the impacts of climate change-induced events (Maximiliano-Cordova et al., 2021; Nehren et al., 2016; Sigren et al., 2014), and foster ecological balance by hosting intricate ecosystems teeming with flora and fauna specialized to survive harsh coastal conditions (Acosta et al., 2005). For example, sand-burial tolerant species like *Ammophila arenaria* (or beachgrass) increases sand accumulation, stabilizes sand and prevents erosion (Gadgil, 2002; Hertling & Lubke, 1999; Hewett, 1970), whereas species less tolerant to burial, such as *Helichrysum stoechas*, are considered to be important in stabilizing low-elevation backdune areas (Acosta & Ercole, 2015) contributing to the overall health of coastal ecosystems. Their ability to dissipate wave energy and reduce coastal flooding not only protects human lives and property but also preserves invaluable coastal habitats and cultural heritage sites. The resilience of coastal dunes in the face of relentless natural disturbances underscores their indispensable role in enhancing coastal resilience and adaptation strategies. Furthermore, coastal dunes hold immense economic value by supporting a wide array of recreational activities, thereby enhancing local tourism industries and regional economies (Pranzini, 2018).

Supervision: M. Piras, C. Camporeale
Validation: D. Demichele
Visualization: D. Demichele
Writing – original draft: D. Demichele
Writing – review & editing: D. Demichele, E. Belcore, M. Piras, C. Camporeale

However, despite their ecological and socioeconomic importance, the dunes are subjected to several threats, from habitat degradation due to invasive species proliferation (French, 2012) to unsustainable human activities. Additionally, climate change-induced alterations like coastal erosion, which is estimated to impact about 70% of the Earth's sandy beach environments and around 42% of Italian sandy coasts (Bertacchi et al., 2016; Martínez et al., 2013). The degradation of coastal dune ecosystems not only compromises their ability to provide crucial ecosystem balance but also increases coastal vulnerability to erosion, flooding, and habitat loss. Thus, it is of paramount importance to improve our knowledge in vegetation spatial patterning in order to address natural-based solutions for coastal management that prioritize their conservation, restoration and sustainable use (Darke et al., 2016; Eamer et al., 2013; Grootjans et al., 2002; Martínez et al., 2013).

The role of vegetation as the primary driving factor for the dynamics of coastal dunes has been established and extensively studied in the last decades (Hesp, 1988, 2002; Short & Hesp, 1982; Walker et al., 2013). As coastal dunes are being either stabilized or mobilized in response to the changes in the rates of sand and dune movement, the vegetation cover and composition are expected to vary, reflecting the differences in the sedimentary conditions (Carter & Wilson, 1993; Muñoz-Reinoso, 2018). Disturbances such as changes in sand supply, intrusion of invasive species (Ciccarelli et al., 2023), and anthropic activities (e.g., agriculture, forestry, infrastructure, urban development and tourist pressure) may modify these fragile spatial patterns (Curr et al., 2000). Dune plant patterns originate as a result of the spatial nature of environmental gradients, processes of succession, or both. It is thus understood that, on one hand, vegetation distribution and biomass depend on several different factors, such as wind exposure (Bressolier & Thomas, 1977), hydrodynamic regimes (Silva et al., 2016), salt spray (Oosting, 1945; Sykes & Wilson, 1988); on the other hand, vegetation characteristics exert a major control on the development of the topographic features mediating these same abiotic governing factors. Hence, these topographic features such as elevation, slope, and distance from the shoreline have been identified as main habitat descriptors for different dune plant species (Durán & Moore, 2013; Kim & Yu, 2009).

The concurrent characterization of vegetation distribution and dune topography has been historically addressed through time-demanding field sampling techniques such as the point count sampling method, transect sampling methods or so-called *quadrant counting methods* (Coulloudon et al., 1999; Frederiksen et al., 2006). Despite their simplicity, these methods are highly subjective because the estimation precision mostly depends on the estimator's experience and cannot be applied to large study areas for practical reasons (Morrison, 2016).

In recent times, remote sensing has provided a comprehensive and cost-effective approach for analyzing vegetation patterns at different spatial and temporal scales, facilitating decision-making for land management, conservation, and environmental monitoring purposes (Chu & Chu, 2020; Xie et al., 2008). The ever-increasing data availability with high spatial and spectral resolution is facilitated using satellite, airborne, and ground-based sensors, which capture information across different wavelengths of the electromagnetic spectrum. A plethora of vegetation indices (e.g., NDVI, NDWI, EVI, MCARI, RI, etc.) can be deducted by multi-spectral imagery to quantify vegetation parameters such as health and density, based on the spectral reflectance (Bermúdez & Retuerto, 2013; Lo & Quattrochi, 2003; Tucker, 1979).

Additionally, machine learning (ML) algorithms have also been applied to remotely sensed data for land cover (LC) analysis (Ahmad et al., 2020; Kattenborn et al., 2021; Martínez Prentice et al., 2021; Nay et al., 2018). Amongst all, Object-Based Image Analysis (OBIA) algorithms have gained popularity for LC classification for their improved accuracy and low sensitivity to noise, compared to other algorithms like pixel-based ones (Berhane et al., 2017; Whiteside et al., 2011). These algorithms can perform segmentation, which partitions images into meaningful segments using algorithms like mean shift or graph-based segmentation and feature extraction to extract spectral, textural, and contextual attributes from segments. Classification algorithms like Decision Trees, Random Forests or Neural Networks are then used to assign to each segment LC classes based on these features. Although these techniques have been successfully applied across various research fields such as forestry, land management, environmental monitoring, and ecological conservation, there remains a notable gap in the literature concerning highly detailed vegetation characterization studies. Specifically, tasks like species identification and biomass density estimation in coastal areas, which often contain small, sparse, and mixed populations of herbaceous plants, are still underrepresented (Silvestri et al., 2003; Yousefi Lalimi et al., 2017). Approaches using OBIA algorithms over Ultra-High Resolution (UHR) imagery, with less than 10 cm spatial resolution acquired through Uncrewed Aerial Vehicles (UAVs), have only been proposed within the last decade and are performed on a multi-temporal scale(Belcore et al., 2021; Michez et al., 2016; Shi et al., 2020). This approach is shown to be

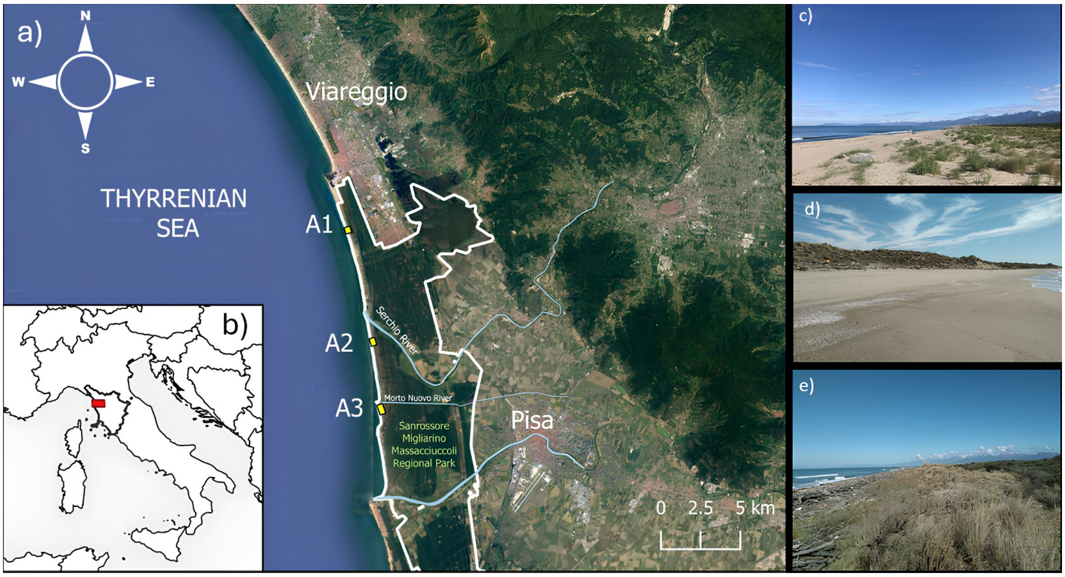

Figure 1. Location of Sanrossore-Migliarino-Massacciuccoli Regional Park (Tuscany, Italy). (a) Full view of the park area (red); (b) Location of the three study areas within the park (yellow points); (c–e) Dunefield picture of A1 (c); A2 (d); A3 (e).

suitable for fine land cover classification in coastal environments, albeit more time and resource demanding than satellite-based image analysis techniques.

In this study, we took advantage of a novel classification model proposed by (Belcore et al., 2024) based on an OBIA algorithm and applied to UHR multispectral UAV imagery to obtain a wide vegetation data set composed of georeferenced and classified polygons at the single-plant level. The present work aims to provide a detailed qualitative and quantitative description of vegetation spatial patterns using statistical and geostatistical tools like spatial correlation (Kim & Yu, 2009; Kowe et al., 2019) and point pattern analysis (Dixon, 2002; Haase, 1995; Pélissier & Goreaud, 2001), well-established for vegetation pattern studies in coastal environments as well as in forests, woodlands and many other environments. Moreover, we combined vegetation distribution studies with topography and hydrodynamic forcings analysis to better understand their effect on each plant species. In particular, the research focuses on examining the following aspects: (a) the interplay of hydraulic forces and the distribution of vegetation; (b) the relationship between topography, vegetation distribution and vegetation geometrical features; (c) the impact of human activities on vegetation distribution, as this park stands out as one of the few dune areas in Italy under complete protection, but still situated close to heavily frequented bathing areas.

2. Material and Methods

2.1. Case-Study

The study site is the Migliarino-Sanrossore-Massacciuccoli Regional Park (Figure 1), covering about 30 km of the Tuscan coastline between Livorno and Viareggio. In 2004, the 23,000 ha park was designated as a Biosphere Reserve by UNESCO (Bertacchi, 2017) for its ecological and landscape value of primary importance. The dune field, in particular, although having a limited extension of about 394 ha, is a scenario of incredible biological richness and diversity and sadly exhibits all the symptoms of climate change and anthropic pressure (e.g., coastal erosion, marine litter deposition, disruption by over-trampling, human-induced dune blowout, sand removal for construction purposes, etc.), even in the 11 km of coastline subjected to protective restrictions (Cipriani et al., 2010). During the last decades, the physical and biological state of the park was subject to constant monitoring by research groups (Alquini et al., 2016; Barducci et al., 2009; Gellini et al., 1983; Leucci et al., 2014; Scopetani et al., 2021) and many interventions of habitat restoration have been successfully attempted (Cipriani et al., 2010).

We focused our attention on three areas of interest along the coastline for a total length of about 1.6 km and approximately 400 m in the cross-shore direction, enough to include the entire dune system that is composed of the shoreline, the foredune, the backdune slack, the fixed dune, and part of the inland pine tree forest.

The first area (430 × 430 m) is located in correspondence with Lecciona Beach (43°49’51”N, 10°15’11”E), a very popular destination for seaside tourism and watersports. The strong impact of anthropic activities prevented the proliferation of psammophytes species, so there is no foredune in this area, instead, there is a series of parallel embryonic dunes, populated by evergreen shrubs and junipers scattered quite homogeneously. The second (500 × 370 m) and third areas (670 × 420 m) are located to the south Serchio River's mouth (43°46’05”N, 10°16’23”E) and to the south of Morto Nuovo River (43°43’48”N, 10°16’41”E), respectively, and they lie inside the restricted area of the park, with little or no direct anthropic impact, although loads of marine litter and woody debris transported by longshore currents can be found on the beach. In these areas, there are the richest communities of psammophyte species and the tallest dunes, which can reach up to 5 m high. Moreover, the shore is not very steep (less than 10°) and thin (less than 20 m at low tide), accentuating the effect of storm-driven overwash and wind erosion on the seaward slope of the foredune, significantly affecting the vegetation zonation.

In all three areas, exotic species like *Yucca gloriosa*, become invasive, displacing local communities, hindering their evolution toward mature stages (Ciccarelli et al., 2023).

The study areas were the subject of a multi-disciplinary monitoring research group since 2021, involving the collection of high-resolution optical data and in-field mapping of more than 900 plant samples. For simplicity, in the following we will refer to the three study areas as A1, A2, and A3.

2.2. Topographic Survey

To obtain a Digital Elevation Model (DEM) of the study areas, an RGB aerial photogrammetric survey has been performed with a quad-rotor DJI Matrice 300 RTK drone equipped with a 45-megapixel DJI Zenmuse P1 camera and a dual-frequency Global Navigation Satellite System (GNSS) to perform Real Time Kinematic (RTK) positioning during the survey carried-out on May 2022. The collected data have been elaborated with a standard Structure from Motion (SfM) workflow in Agisoft Metashape software to generate DEMs up to 3 cm resolution ($2 \cdot 10^4$–by–$2.2 \cdot 10^4$ pixels, on average). Terrain models have been georeferenced in the WGS84-UTM 32N coordinate system through direct photogrammetry. The position of 9 markers for each area has been measured using a GNSS receiver in RTK mode to check the precision of the output DEM. The elevation of these markers is then converted from ellipsoidal to orthometric utilizing geoid undulation values supplied by the Italian government. The DEMs of the study areas have been processed in QGIS environment to generate Digital Terrain Models (DTM), shown in Figure 2 according to the following procedure: (a) A slope-based SAGA-GIS DTM filter has been applied to DSMs (Vosselman, 2000) to remove objects and vegetation features. (b) A multilevel B-Spline interpolation SAGA-GIS algorithm (Lee et al., 1997) has been used to fill the gaps in the filtered DEMs.

2.3. Runup Computation

The effect of the hydrodynamic forcing on the vegetation has been addressed through an analysis of the wave runup, namely, the maximum elevation gain reached by the water on the shoreline. The elevation gain is due to the conversion of part of the kinematic energy of the wave into potential energy (Hunt Jr, 1959).

For this analysis, data have been collected from the National wave-metric and tide-gauge network open database, run by the Italian Institute for Environmental Protection and Research (ISPRA). We retrieved the time series of the spectral significant height H_0 and the spectral peak period T_p over 30 min of deep water waves collected by the wave buoy of La Spezia and the time series of mean water levels η collected by the hydrometer of Livorno, with a sampling period of 10 min. The time span of collected data is from 01/06/2021 to 31/12/2022 (the original data set is available on https://www.mareografico.it).

For the computation of the runup we adopted the model proposed by Stockdon et al. (2006).

$$R_u = (H_0 L_0)^{1/2}\left[0.385\beta_f + \left(0.17\beta_f^2 + 0.0012\right)^{1/2}\right], \tag{1}$$

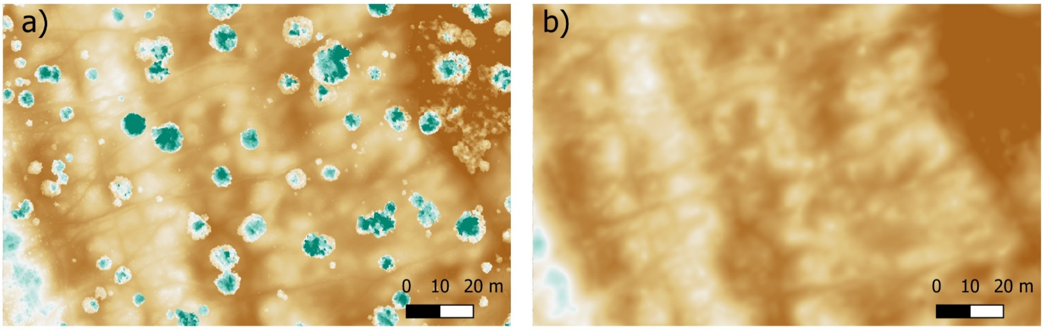

Figure 2. Example of generation of Digital Terrain Model (DTM) (b) from a Digital Surface Model (DSM) (a) for the area A1.

where L_0 is the spectral significant wavelength in deep waters, defined by the dispersion relation $L_0 = gT_0^2/2\pi$; T_0 is the spectral significant wave period in deep waters, defined by $T_0 = 0.95T_p$, where T_p is the peak spectral period; β_f is the beach steepness, that is, the tangent of the slope angle of the water's edge, θ (Figure 3). An average β_f has been calculated for each study area by extracting from the DTMs 100 equally spaced transects perpendicular to the shoreline and computing for each one the beach steepness $\beta_f = \langle 2/(x_2 - x_i) \rangle$, where x_0 and x_2 are the coordinates in the cross-shore direction of points at elevations 0 and 2 m above sea level, respectively (Figure 3a). This choice is justified by the fact that the region between 0 and 2 m elevation lies within the shoreline and the foredune toe and the slope is steady. Total water level h is then computed as the sum of the mean sea level η and the runup R_u, namely $h = \eta + R_u$.

2.4. Vegetation Pattern Classification

The starting point of the present study on the vegetation pattern is a field-based data set derived from the object-based image analysis (OBIA) recently proposed by our research group (Belcore et al., 2024). The algorithm has been trained to detect and classify 12 different plant species, as well as sand and debris (as listed in Table 1), with an average accuracy of 75%, in line with similar studies in forest or riparian environments (Michez et al., 2016; Shi et al., 2020). The output data set is composed of a shapefile containing more than 600,000 polygons, each one representing the canopy cover of the single plant, that is, the area covered by the vertical projection of the outermost perimeter of the natural spread of foliage of plants (Coulloudon et al., 1999). Each polygon is then labeled with an abbreviation of the object class name. The reader may refer to (Belcore et al., 2024) for further details about the classification technique. Morphometric parameters of the polygons, such as the coordinates of the centroids, areas, and perimeters have been extracted using QGIS.

Since Juniperus shrubs and Pine trees predominantly constitute the backdune vegetation patch, a first cleaning of the data set removed all the polygons corresponding to these species. Then, all the polygons with an area less than 0.01 m^2 have been removed.

The abundance of each plant species in each study area has been computed as the ratio between the number of elements of a single species and the total number of plants in the whole area (Kim & Yu, 2009). Species having an abundance of less than 1% has been considered not statistically relevant and therefore, neglected in successive analysis.

To support some of the key results, we implemented a two-dimensional visualization of the spatial distribution of the vegetation in the form of vegetation cover maps, as shown in the example in Figure 3b. The complete set of ground cover maps for the sites A1–A3 are reported in the Figures S1–S3 of Supporting Information S1. After subdividing the study area with a 5 m equally spaced grid, the vegetation cover $\psi_{i,j}$ has been computed for each cell defined as the ratio between the total area of the polygons of the i-th plant species inside the j-th cell and the area of the cell itself, namely $\psi_{i,j} = A_i^{veg}/A_j^{cell}$, where A_i^{veg} is the area of a segmentation polygon (or a portion of polygon) of the i-th plant species and A_j^{cell} is the cell area. A scheme for the computation of $\psi_{i,j}$ is represented in Figure 4a.

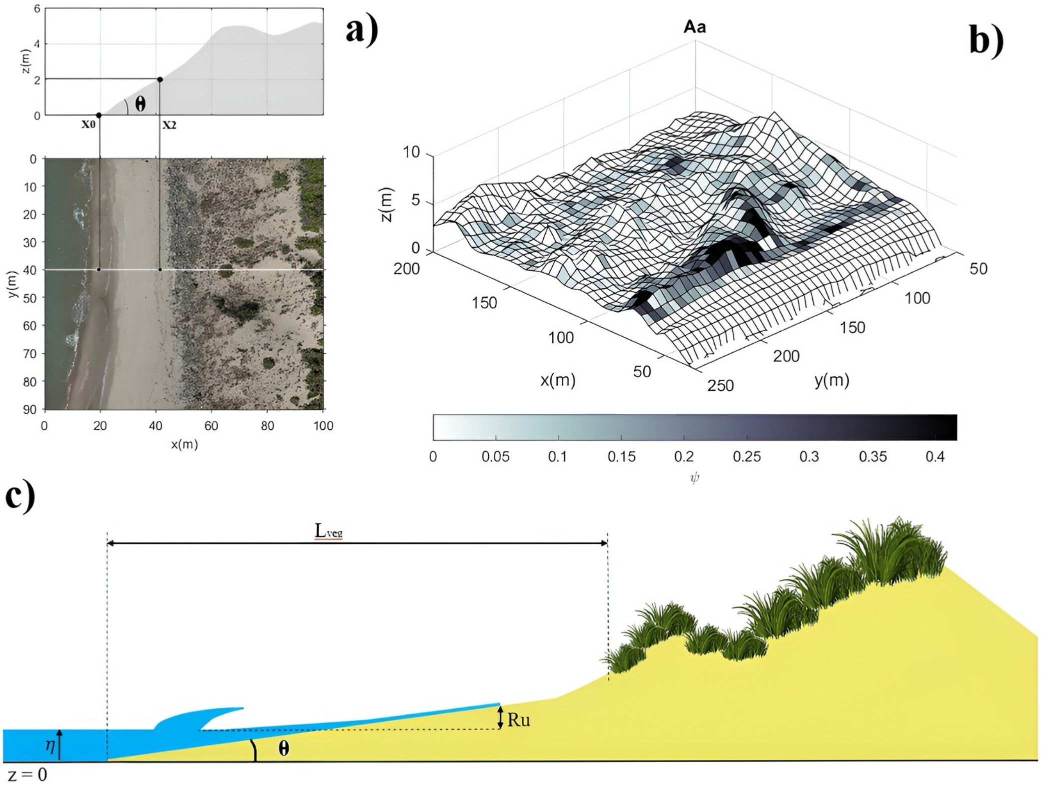

Figure 3. (a) Example section (top) extracted from the Digital Terrain Model (DTM) used to compute $\beta_{f,i}$. The orthoimagery (bottom) highlights a transect marked by a solid white line, with points at elevations of 0 and 2 m indicated. (b) Two-dimensional vegetation cover map of Ammophila arenaria in A3 with 5 m resolution, overlaid on the DTM of the study area. The shading of each cell represents the corresponding ψ value. (c) Geometric configuration of the considered beach-dune profile. The sea water level h is the sum of wave runup R_u (function of the beach slope θ) and the mean water level fluctuation due to tides η. Because of marine disturbance, vegetation can grow only beyond the threshold distance L_{veg} from the shoreline.

2.4.1. Geometric Indices

To analyze vegetation patterns, we used morphometric indicators focused on plant size and local spatial density. Plant size was quantified using the equivalent diameter (ED), defined as the diameter of a circle with the same area as the plant's canopy cover (Figure 4b) (Schandry & Becker, 2020), namely

$$\mathrm{ED} = 2\sqrt{\frac{A_i^{veg}}{\pi}}. \tag{2}$$

The local spatial density is instead represented by the Mean Neighbor Distance (MND), namely the mean distance of the centroid of an individual plant from its neighbor plants of the same species. Neighboring points are defined as connected nodes in a two-dimensional first-order Delaunay triangulation network (Joshi et al., 1997)

$$\mathrm{MND}_i = \frac{1}{m}\sum_{j=1}^{m} t_{i,j}, \tag{3}$$

where $t_{i,j}$ is the Euclidean distance between a nodes i and j of the Delaunay triangulation network, and m is the number of nodes connected to the node i (Figure 4c). Triplets of points constituting the network meshes have been computed with the MATLAB *Delaunay* function.

Table 1
List of Plant Species Detected by the OBIA Algorithm, Along With Their Name Abbreviation and Phytosociological Role

Plant species	Abbreviation	Role
Achillea maritima (L.) Ehrend. and Y.P.Guo	Am	Pioneer
Dittrichia viscosa (L.) Greuter	Dv	Pioneer
Echinophora spinosa L.	Es	Pioneer
Eryngium maritimum L.	Em	Pioneer
Euphorbia paralias L.	Ep	Pioneer
Helycrisum stoechas (L.) Moench	Hes	Pioneer
Pancratium maritimum L.	Pm	Pioneer
Ammophila arenaria (L.) Link	Aa	Dune-building
Daphne gnidium L.	Dg	Evergreen
Juniperus oxycedrus L.	Jo	Evergreen
Pinus pinaster Aiton	Pp	Evergreen
Yucca gloriosa L.	Yg	Evergreen

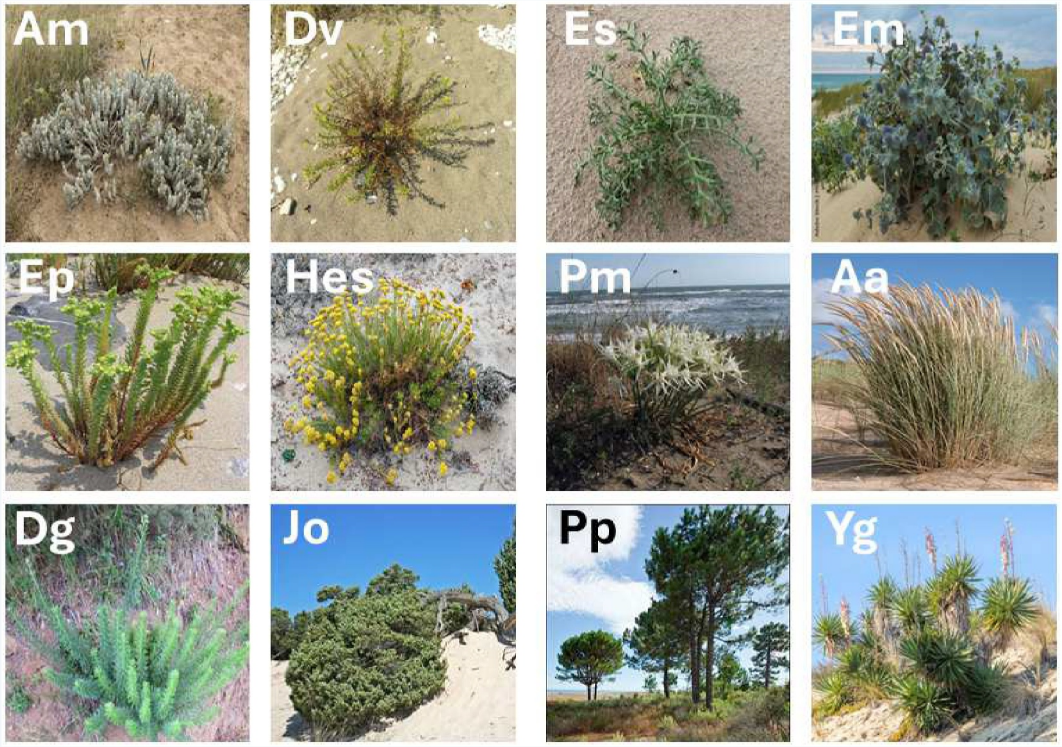

2.4.2. Spatial Autocorrelations

The spatial autocorrelation of ED and MND has been addressed through a geostatistical analysis by using semivariograms. The semivariance $\gamma(h)$ is defined as the half the average of the squared differences between values assumed by a spatially distributed quantity, Z, at locations x_i and x_j separated at distance h (Matheron, 1963). When dealing with field measurements, Z is a discrete quantity and not a continuous field, so we consider the set of all the pair of points whose distance is within $h + \frac{\delta}{2}$ and $h - \frac{\delta}{2}$, where δ is an suitable bin width.

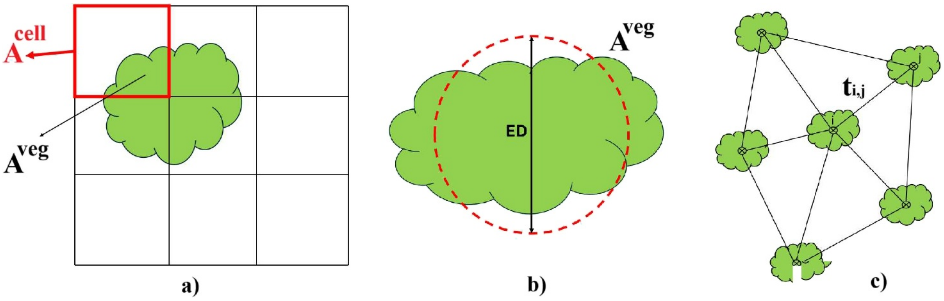

Figure 4. Scheme for calculating: (a) Vegetation Cover: the ratio between the area of the plant's polygon within a cell $\left(A_i^{veg}\right)$ and the area of the cell itself $\left(A_j^{cell}\right)$ (red square). (b) Equivalent Diameter (ED): the diameter of a circle (red dotted line) with the same area as the plant's polygon $\left(A_i^{veg}\right)$. (c) Mean Nearest Distance (MND): the centroid of each polygon representing a single plant (black circle with an "x"), with centroids connected by a Delaunay triangulation network (black lines). $t_{i,j}$ are the lengths of the network links.

$$\gamma(h) = \frac{1}{\sigma_Z^2}\frac{1}{2\left|n\left(h \pm \frac{\delta}{2}\right)\right|}\sum_{(i,j)\in n\left(h\pm\frac{\delta}{2}\right)} |Z_i - Z_j|^2. \tag{4}$$

In the above equation, the semivariance has been normalized with the variance of Z, eliminating scale effects, to compare different semivariograms.

The spatial structure of the geometric features of vegetation was identified by fitting the experimental semivariograms onto four widely used semivariogram models: (a) Gaussian: $\gamma(h) = d + C\left(1 - e^{-h^2/a^2}\right)$; (b) Exponential: $\gamma(h) = d + C\left(1 - e^{-h/a}\right)$; (c) Spherical: $\gamma(h) = d + C\left(\frac{3}{2}\frac{h}{a} - \frac{1}{2}\frac{h^2}{a^2}\right)$; (d) Pure nugget: $\gamma(h) = d$.

In these models, C is the *sill* (i.e., the theoretical limit of γ for $h \to \infty$, equal to the variance of Z if it is randomly distributed in space), d is the *nugget* (i.e., the height of the jump of the semivariogram at the discontinuity at the origin), and a is the range (i.e., the value of h for which the difference between the sill and the semivariogram is negligible and roughly corresponds to the integral length scale at which Z loses spatial correlation with itself). For a sensible autocorrelation analysis, we neglected semivariograms showing (a) too-low coefficient of determination, $R^2 < 0.7.$; (b) too-high noise level, $d > 0.9$; (c) unclear structure, $C - d < 0.1$.

2.4.3. Point Pattern Analysis

The characterization of vegetation spatial arrangements has been performed using point pattern analysis. Point pattern analysis methods fall into two predominant categories: (a) nearest neighbor-based and (b) distance-based methodologies. The former centers around nearest neighbor distance, denoting the minimum distance between one element and another within the population, while the latter is based on the enumeration of elements contained within a specified distance.

The mean nearest neighbor (MNN) method is based on the nearest neighbor distance $\overline{d_o}$, denoting the minimum distance between two a zero-dimensional objects within a population (Sadahiro, 2024):

$$\overline{d_o} = \frac{1}{N}\sum_{i=1}^{N} \min(d_{i,j}), \tag{5}$$

where $\min(d_{i,j})$ is the distance of a given event i to its closest neighbor and N is the size of the sample taken into the exam. For comparison purposes, we will refer to the case of a random distribution of points, in the following referred to as Complete Spatial Randomness (CSR), which is originated by a homogeneous Poisson process, namely, the probability of finding a number k of points in a region randomly chosen within the study area follows the Poisson distribution. In the case of CSR, the expected value of the MNN is $\overline{d_e} = \sqrt{\rho}/2$, where $\rho = N/A$ is the number of points per unit area and A is the study area (P. Clark & Evans, 1954).

The nearest neighbor index (NNI) refers to the ratio $r = \overline{d_o}/\overline{d_e}$, and represents a measure of the departure from a random distribution of a set of points. Therefore the spatial arrangement is clustered if $r < 1$, or uniformly dispersed if $r > 1$. The reliability of the prediction of the spatial pattern through the NNI is assessed by statistically testing the departure of the null hypothesis, that is, the CSR. The testing variable in this case is the standardized mean nearest neighbor which follows a standardized normal distribution (P. Clark & Evans, 1954):

$$Z = \frac{\overline{d_o} - \overline{d_e}}{\sigma_{\overline{d_e}}}, \tag{6}$$

where $\sigma_{\overline{d_e}} = 0.261/\sqrt{\rho N}$ is the standard deviation of nearest neighbor distances in the case of CSR (P. Clark & Evans, 1954). We choose a double-tailed test with a 95% confidence interval to test the departure from the null hypothesis. To indicate a statistically significant clustering or dispersion of the observed point pattern, the value of Z must be less than -1.96 –indicating clustering– or greater than 1.96 –indicating dispersion–. The values $Z = -1.96$ and $Z = 1.96$ respectively correspond to the 2.5th and the 97.5th percentile of the distribution of Z.

In addition, Ripley's K-function $K(r)$ has been used to perform a distance-based point pattern analysis. It measures the average number of points that fall within a circle of a given radius r centered on each point of the population (Ripley, 1984)

$$K(r) = \frac{1}{N}\frac{1}{\rho}\sum_{i}\sum_{j\neq i} I(d_{i,j} < r)\, w(x_i, x_j), \tag{7}$$

where: ρ is the number of points per unit area, N is the size of the sample, $I(r_{i,j} < r)$ is the indicator function (Dixon, 2002) ($I = 1$ if the distance between points i and j is less than r and assumes value $I = 0$ otherwise), $w(x_i, x_j)$ is Ripley's edge-effect correction factor (Goreaud & Pélissier, 1999), wherein $w = 1$ if the circle centered in x_i with radius r lies completely within the study area, otherwise w assumes a value less than 1, equal to the ratio between the total circumference of the circle of radius r and its sector inside the study area.

The edge effect is more significant at greater values of r because the research circle is more likely to fall partially outside the study area. Similarly to the Nearest Neighbor method, the type of spatial arrangement can be identified by comparing the observed K-function with its expected value in the case of CSR, equal to πr^2. Therefore, $K(r) > \pi r^2$ indicates a clustered pattern, and $K(r) < \pi r^2$ indicates a uniformly dispersed pattern.

Both the expected and observed K-function increase with the square of the distance, and, at higher values of r, small differences in the spatial arrangement of points become barely distinguishable. To circumvent such a scale-effect problem, Besag and Diggle (1977) suggested the use of a modified version of the K-function, the L-function, expressed as follows:

$$L(r) = \sqrt{\frac{K(r)}{\pi}} - r, \tag{8}$$

whose the expected value for the CSR case is $L = 0$. It follows that positive values of the observed $L(r)$ indicate clustering, otherwise, negative values indicate dispersion.

As evidenced by Kiskowski et al. (2009), in the case of a clustered point pattern, the value of r at which occurs the maximum of the observed $L(r)$ gives a slight overestimate of the radius of the clusters. Although the L-function can provide an initial assessment of whether the observed point pattern differs from complete spatial randomness, it's unclear how much the observed function should deviate from its expected values (e.g., zero for the L-function) to indicate significant clustering or dispersion in a statistical sense. For this study, we used a Monte Carlo simulation approach to build the confidence envelope of the CSR hypothesis. A number m of samples composed by N points (10^4 in our case) are randomly placed within the study area. $L_{i,i=2,\ldots,m}(r_j)$ is computed for various distances r_j for each i-th sample and sorted in ascending order. The 95% confidence interval limits are given by the

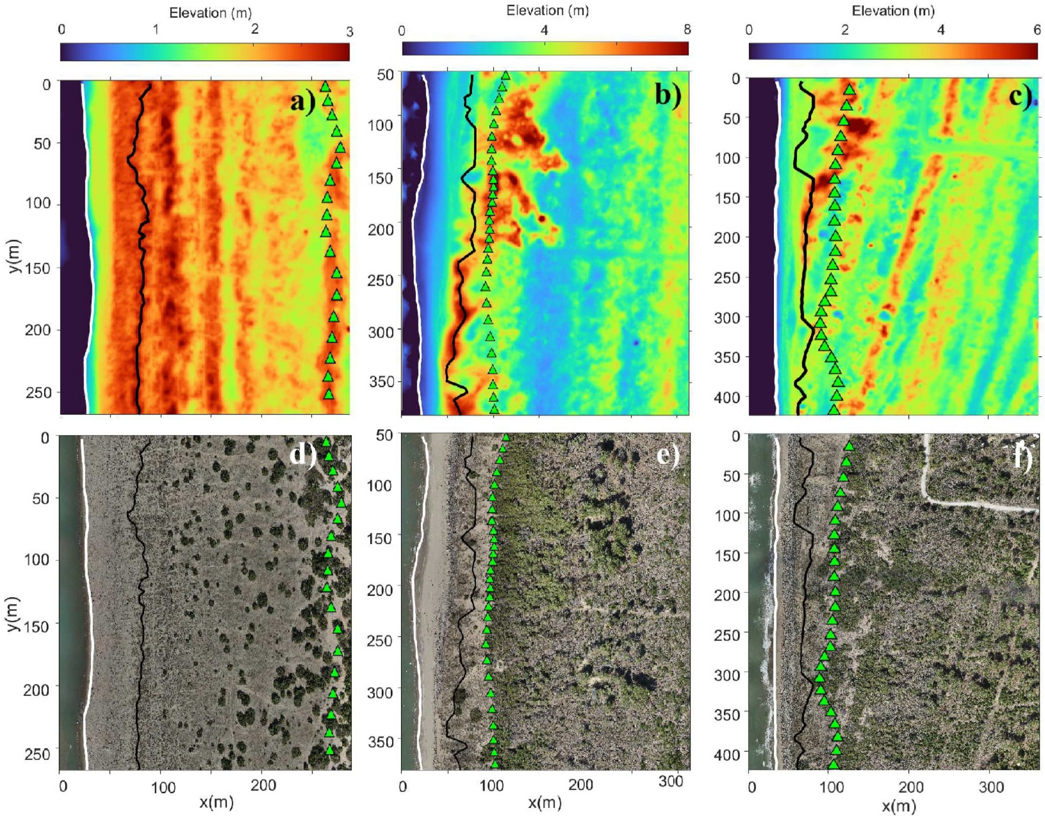

Figure 5. DTMs of areas A1(a), A2(b) and A3(c). The shoreline (white line), the foredune crestline (black line), and the limit of the patch of tree vegetation (green triangles) are also reported. Orthoimagery of A1(d) A2(e) and A3(f) are portraited for visual comparison with DTMs.

250th and the 9750th largest value of $L(r_j)$, corresponding to the 2.5th and 97.5th percentile of the distribution of $L(r_j)$. Repeating this procedure for each distance r_j, the 95% confidence envelope is therefore constructed (Myllymäki et al., 2017). A statistically significant clustering (or dispersion) is determined whereas the observed L-function lies above (or below) the confidence envelope.

Table 2

Abundance of Plant Species Expressed as the Ratio Between the Number of Elements of a Single Species and the Total Amount of Plants Detected in the Three Study Areas

	Aa	Em	Ep	Es	Hes	Pm	Dg	Yg
A1	0.05	0.23	0.04	0.44	0.12	0.09	–	0.01
A2	0.34	0.07	0.28	–	0.19	0.03	0.09	0.0005
A3	0.41	0.006	0.05	0.0001	0.32	0.0002	0.12	0.07

Note. Cells are colored with a gradient of abundance from red to green to visually enhance the comparison between values. (*Aa, Ammophola Arenaria; Em, Eryngium Maritimum; Ep, Auphorbia Paralias; Es, Echinophora Spinosa; Hes, Helichrysum Stoechas; Pm, Pancratium Maritimum; Dg, Daphne Gnidium; Yg, Yucca Gloriosa*).

3. Results and Discussion

3.1. Overview of Dune Morphology and Biogeography

Upon initial examination of the digital terrain models (DTMs) within the study areas, three distinct structures that characterize the dune systems become evident (see Figure 5). Area A1 stands out from the other two due to anthropogenic disturbances. It consists of multiple bands of embryonic dunes running parallel to the shoreline, spaced approximately 25–30 m apart, with a height not exceeding 70–80 cm. This is reflected in the limited proliferation of dune-building species, such as *Ammophila arenaria*, in this environment, as their presence is notably scarce compared to A2 and A3, where they are more abundant (see Table 2).

Area A2 exhibits the characteristic structure of a mature coastal dune, featuring a well-developed foredune primarily colonized by ammophyte species, which can attain heights of up to 8 m. It also includes a humid backdune slack and a fixed dune with patches of coniferous plant species like *Pinus Pinaster*. In contrast, despite being within the confines of the Regional

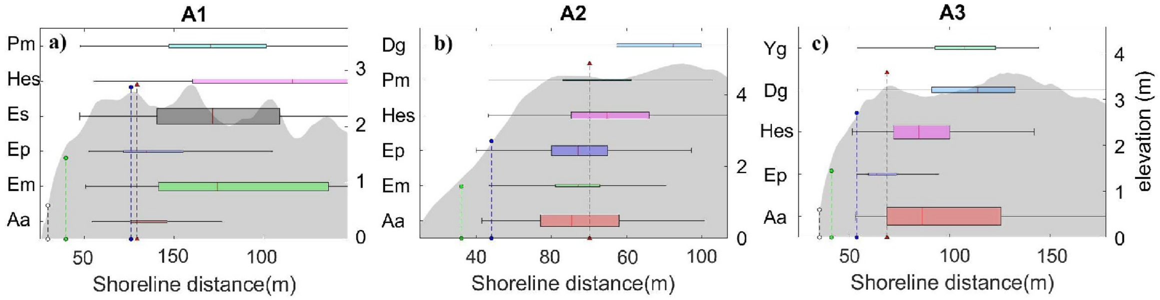

Figure 6. Boxplot depicting the species spatial distribution of plant species and the mean topographic profile (depicted in gray) along the cross-shore direction for A1 (a), A2 (b) and A3 (c). The width of the boxes corresponds to the abundance of the species within the study area. Additionally, the positions of the mean foredune crest (black dashed line with red triangles), mean total water level (blue dashed line with blue dots), 95th percentile (green dashed line with green dots), and 99th percentile (black dashed line with white dots) are highlighted. (Abbreviations: *Aa, Ammophila arenaria; Em, Eryngium maritimum; Ep, Euphorbia paralias; Es, Echinophora spinosa; Hes, Helichrysum stoechas; Pm, Pancratium maritimum; Dg, Daphne gnidium; Yg, Yucca gloriosa*).

Park like A2, Area A3 displays a different structural pattern. The orientation of its dune bands deviates approximately 17° from alignment with the shoreline (see Figure 5c), influenced by ongoing coastal erosion attributed to the proximity of the Morto Nuovo river outlet (Pranzini, 2018). In this area, a nascent system of foredunes is emerging, though still in the process of formation. Consequently, it presents a more rugged structure and a lower crestline elevation compared to the foredunes of A2.

A notable distinction between A1 and A2–A3 lies in the width of the coastal zone colonized by shrub and herbaceous species, delineated as the distance between the shoreline and the vegetative cover. In A2 and A3, this distance measures approximately 70–80 m, whereas in A1, it extends to about 250 m, as illustrated in Figures 5a–5c.

In A2 and A3, foredunes exhibit significant development, attaining elevations of 5–6 m. The barrier effect of these dunes engenders marked variations in wind exposure, influencing abrasive forces, nutrient dispersion, and moisture levels (Kim & Yu, 2009). These pronounced gradients in environmental conditions manifest in the spatial distribution of plant species across distinct morphological units of the dune system (e.g., foredune, slack, secondary dune, etc.), contingent upon their ecological tolerance levels. An exemplary demonstration of the tight coupling between terrain morphology, environmental gradients, and plant zonation is observed in halophytic species, such as *Ammophila arenaria* and *Euphorbia paralias*. These species predominantly populate the vicinity surrounding the crest of the foredune (as depicted by the distribution of *Aa* and *Ep* in Figures 6b and 6c). Conversely, species like *Helichrysum stoechas* and *Daphne gnidium*, which thrive in more moisture-rich habitats and are shielded from adverse environmental stressors, are primarily situated within dune slacks and stabilized dune formations (refer to the distribution of *Hes* and *Dg* in Figures 6b and 6c).

Conversely, in A1, the predominantly flat terrain results in a notably less pronounced gradient of environmental factors, yielding a vegetation zonation that is more diffuse and less distinct. Indeed, across the entire area, species exhibit a more homogeneous distribution pattern. This is evident in the interquartile ranges (IQRs) and whiskers depicted in the boxplots presented in Figure 6a, which illustrate the spatial distribution of vegetation species. Notably, these boxplots show significantly wider IQRs and whiskers in comparison to those observed in A2 and A3 (see Figures 6b and 6c).

In A2 and A3, the narrowness of the shore precludes the formation of embryonic dunes on the seaward side of the foredune, largely due to limited space exacerbated by accumulations of wooden debris. Consequently, the scarcity of vegetation species typical of embryonic dunes, such as *Eryngium maritimum*, *Echinophora spinosa*, and *Pancratium maritimum* (Acosta & Ercole, 2015), mirrors the morphology of these areas, which lack embryonic dune structures. Conversely, these species thrive in A1, where the terrain primarily comprises embryonic dunes.

Another notable difference in vegetation distribution between A1 and the other two areas involves *Daphne gnidium*, a species typically associated with fixed dunes and dune slacks, along with Juniperus shrubs or Pine trees (Acosta & Ercole, 2015). In A1, where fixed dunes are absent, *Daphne gnidium* is scarce, contrasting with its presence in A2 and A3. This pattern aligns with the distribution of Juniperus, sparsely scattered from the shoreline to the patch of tree vegetation.

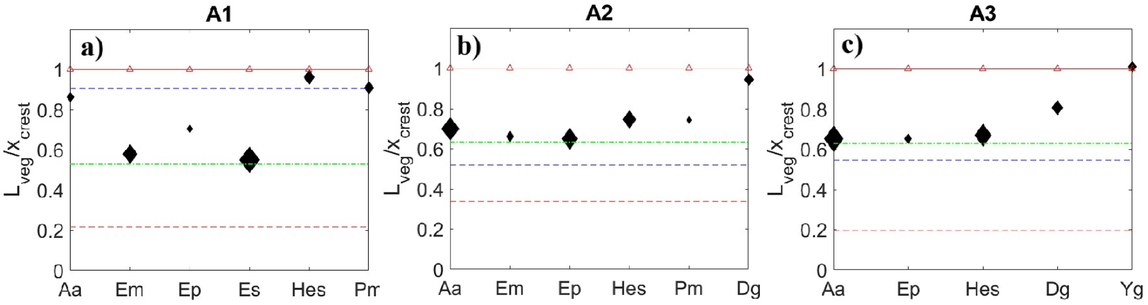

Figure 7. Plots of normalized L_{veg} for different plant species. The size of the diamonds is proportional to the abundance of each species. The plots highlight the mean distances from the shoreline of the 95th (red dotted line) and 99th (blue dotted line) water level contour lines, the mean overall threshold vegetation line (green dotted line), and the crestline (red triangles). (Abbreviations: *Aa, Ammophila arenaria; Em, Eryngium maritimum; Ep, Euphorbia paralias; Es, Echinophora spinosa; Hes, Helichrysum stoechas; Pm, Pancratium maritimum; Dg, Daphne gnidium; Yg, Yucca gloriosa*).

Helichrysum stoechas, a species favored in areas sheltered from direct onshore winds and waves, exhibits similar abundances across all three areas (see Table 2). In A2 and A3, it primarily occupies the landward slope of the foredune and the dune slack (see Figures 6b and 6c), whereas in A1, it proliferates not only in such sheltered areas but also between the second and fourth rows of embryonic dunes (illustrated by the boxplot of *Hes* in Figure 6a).

3.2. Thresholds

The literature extensively underscores the significance of a critical threshold distance from the shoreline, commonly denoted as L_{veg}, beyond which vegetation survival becomes viable (Durán & Moore, 2013). This threshold delineates a zone where environmental forces exceed levels conducive to vegetation encroachment (see Figure 3c). L_{veg} holds particular importance in coastal ecomorphodynamic modeling, serving as a pivotal determinant for vegetation colonization and thus exerting control over the dune-building process.

Figure 7 illustrates the ratio between the average overall L_{veg} and the mean distance of the foredune crestline from the shoreline x_{crest}, which consistently remains around 0.6 across the three areas, specifically 0.62 for A2 and A3, and 0.54 for A1. Hence, this ratio appears minimally influenced by terrain morphology. Nonetheless, further case studies are necessary to extend the applicability of this finding. The L_{veg}/x_{crest} ratio has been calculated individually for each plant species (Figure 7).

Species shared between A2 and A3, namely *Ammophila arenaria*, *Euphorbia paralias*, *Helichrysum stoechas*, and *Daphne gnidium*, display consistency in their respective L_{veg}/x_{crest} values, regardless of their abundance. Coherently with their zonation, halophyte species, proliferating closer to the coastline, exhibit L_{veg} values closely aligned with each other and with the overall L_{veg} (Figures 7b and 7c). In A1, L_{veg}/x_{crest} values for individual species are inconsistent with those found for the same species in A2 and A3 (Figures 7b and 7c). For instance, *Ammophila arenaria* and *Euphorbia paralias* respectively display L_{veg}/x_{crest} ratios of about 0.9 and 0.7 in A1 (Figure 7a), contrasting with values around 0.63 observed in A2 and A3.

Despite these discrepancies, some similarities are remarkable: (*a*) L_{veg} of halophyte species such as *Eryngium maritimum* and *Echinophora spinosa*, abundant in A1, overlaps with the overall L_{veg} (Figure 7a), akin to observations in A2 and A3 (Figures 7b and 7c); (b) L_{veg} of *Ammophila arenaria*, scarce in A1 but abundant in A2 and A3, closely aligns with the h_{99} line (Figure 7a), resembling trends observed in A2 and A3 (Figures 7b and 7c). This correlation suggests that flooding may be the primary determinant of L_{veg} for *Ammophila arenaria*, while not necessarily for other halophytes.

3.3. Effects of Wave Forcing on Vegetation Boundaries

In the present study, a preliminary assessment of wave runup has been conducted by using Stockdon's empirical model (Equation 1), as a simplified function of the beach steepness, to examine the interaction between hydrodynamic forcing and vegetation. A more advanced wave modeling analysis guided by computational fluid

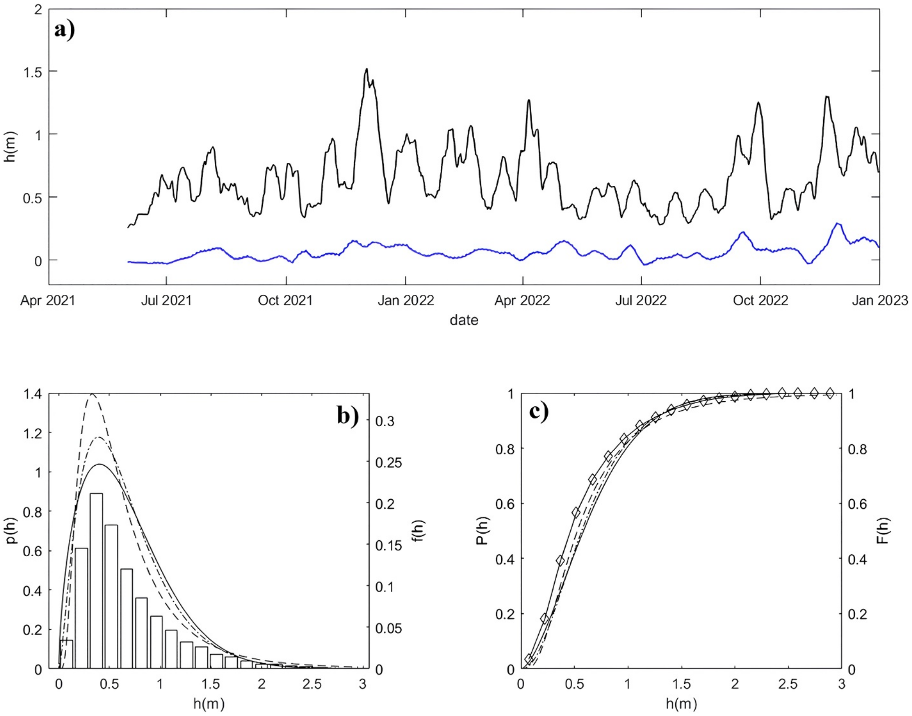

Figure 8. (a) Time series of the mean sea level η from RMN database (blue line) and total water level h for $\beta_f = 0.11$ (black line). (b) PDF of Lognormal (dashed lines), Gamma (dot-dashed line), Weibull (solid line), and histogram of the observed sample. (c) CDF of Lognormal (dashed lines), Gamma (dot-dashed line), Weibull (solid line) and observed CDF (solid line with diamonds).

dynamics (CFD) approaches (e.g., Delft3D software) will be adopted in forthcoming works. The average steepness for A1, A2, and A3 results in 0.136, 0.075, and 0.127, respectively. Since the mean total water levels associated with these three different values differ among each other by less than 10 cm, for simplicity, a mean value of $\beta_f = 0.11$ has been assumed for all the areas, with the resulting mean total water level $h_m = 0.65$ m. Accordingly, the whole time series of the mean sea level and the total water level is reported in Figure 8.

The best fitting of the probability distribution function of h was evaluated by using the χ^2 test and by minimizing the RMSE between the theoretical and observed cumulative distribution functions (CDFs). We set a significance level of $\alpha = 5\%$ and used $k = 20$ classes, resulting in a degree of freedom $l = k - n_p - 1$, where n_p represents the number of parameters for a given distribution. We considered three distinct two-parameter distribution models: Lognormal, Gamma, and Weibull. As reported in Figures 8b and 8c (see also Table S1 in Supporting Information S1), all three distributions are well fitted onto the sample data (low p-values for χ^2 test and low RMSE). The Lognormal distribution emerged as the most statistically robust choice, so it was adopted to compute three characteristic values: the mean total water level, the 95th percentile, and the 99th percentile, respectively equal to 0.52, 1.63, and 2.61 m. For ease of reference, we will denote these water levels as h_{50}, h_{95}, and h_{99}.

Figure 9 shows a comparison between the vegetation threshold line L_{veg} and contour lines of elevations corresponding to h_{95} and h_{99}, which mark the limits of the flooded areas on the shore. Instead, the shoreline has been computed as the contour line of the DTM corresponding to 0 m elevation on the mean sea level.

In the areas A2 and A3 (Figures 9b and 9c), h_{99} corresponds to the front edge of the foredune and almost overlaps with the L_{veg} edge, which is slightly higher elevation and closer to the crestline (the average distance between the two lines is approximately 5.7 and 2.8 m, for A2 and A3, respectively). Therefore, exposure to waves during severe autumnal and winter storms prevents the growth of any type of vegetation, acting like a cut-off for vegetation zonation. On the contrary, in area A1, the h_{99} line reaches past the L_{veg} border, actually interacting with the vegetation which is very sparsely distributed on the seaward side of the first dune crest.

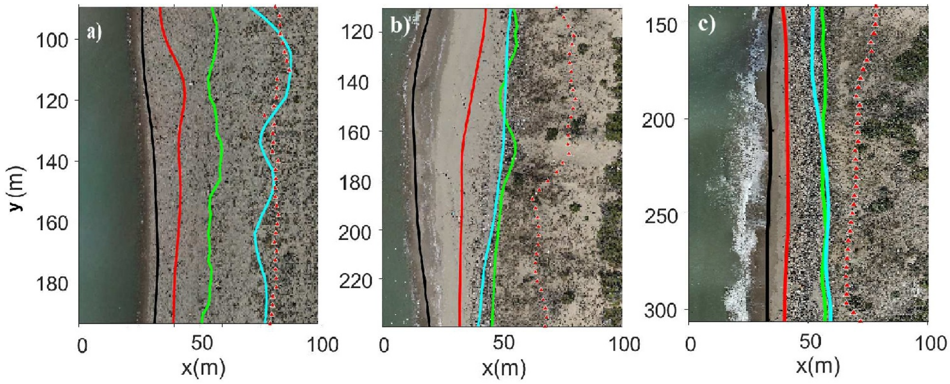

Figure 9. Orthoimages of A1(a), A2(b), A3(c) with contour lines corresponding to 0 m elevation, marking the reference shoreline position (solid black line), 95th (solid red line) and 99th (solid cyan line) total water level percentile. Overall vegetation threshold line (solid green line) and foredune crestline (red triangles) are also highlighted.

3.4. Geometrical Features

The computation and distribution of the Equivalent diameter (ED, cfr. Equation 2) is reported in Figures 10a–10c. The statistical distributions of the same species in different areas are coherent with each other, as shown by the similarity of boxplots (in terms of median and IQR) of *Aa, Em, Ep, Pm, Dg* in Figures 10a–10c. This suggests that different morphology, environmental conditions and abundance do not significantly affect the size distribution of vegetation species. The main exception is *Helichrysum stoechas*, which measures 0.27 m in A1, notably less than the 0.4–0.5 m in A2 and A3. This could be due to either: (a) its concentration in heavily trodden areas of A1, leading to more anthropogenic impact, or (b) heightened inter-species competition since species are evenly spread in A1, resulting in fewer resources per species. A significant 30% decrease in *Helichrysum stoechas* distribution across the shore (from 0.35 to 0.25 m) around 40 m behind the initial crestline may mark where overtrampling effects intensify.

Figures 10d–10f illustrate a consistent trend in the spatial distribution of ED among all species, namely a notable decline as the distance from the peak point increases. Notably, *Ammophila arenaria* in A2 and A3 bucks this trend, maintaining relatively stable ED regardless of distance from the shoreline. Moreover, in A1, where wave runup extends beyond the vegetation threshold, ED diminishes rapidly toward the swash zone, particularly between the 95th and 99th percentile line (Figure 2a). This underscores how severe flooding events impede plant growth, hindering their size.

Figures 11a–11c illustrates the remarkable variability of the Mean Neighbor Distance (MND) across three study areas, contrasting with the Equivalent Diameter (ED) patterns. In A1, species exhibit notably wider intra-species distances, with median values surpassing 2 m, observed in species like *Euphorbia paralias*, *Helichrysum stoechas*, and *Pancratium maritimum*. Conversely, A2 and A3 show consistent MND distributions among shared species, with narrower intra-species distances, generally below 2 m.

Interestingly, species with lower abundance tend to display wider Interquartile Ranges (IQRs) and higher medians across all areas. This suggests that abundance influences not only average spatial density but also spatial distribution patterns. Narrow IQRs indicate more uniform spacing, while wider IQRs suggest a more irregular, patchy distribution.

Less abundant species, as the cases of *Ammophila arenaria* and *Euphorbia paralias* in A1 (Figure 11a), *Eryngium maritimum* and *Pancratium maritimum* in A2 (Figure 11b), and *Euphorbia paralias* and *Daphne gnidium* in A3 (Figure 11c), with high IQR, show a decrease of MND within a short distance from the minimum, indicating a "quick" spread out from the region of maximum density. Instead, more abundant species like *Echinophora spinosa* in A1 (Figure 11a), *Ammophila arenaria*, *Euphorbia paralias*, and *Helichrysum stoechas* in A2 (Figure 11b), and *Ammophila arenaria* and *Helichrysum stoechas* in A3 (Figure 11c), also tend to spread out with distance from the peak density region, but to a much lesser magnitude and within wider distances.

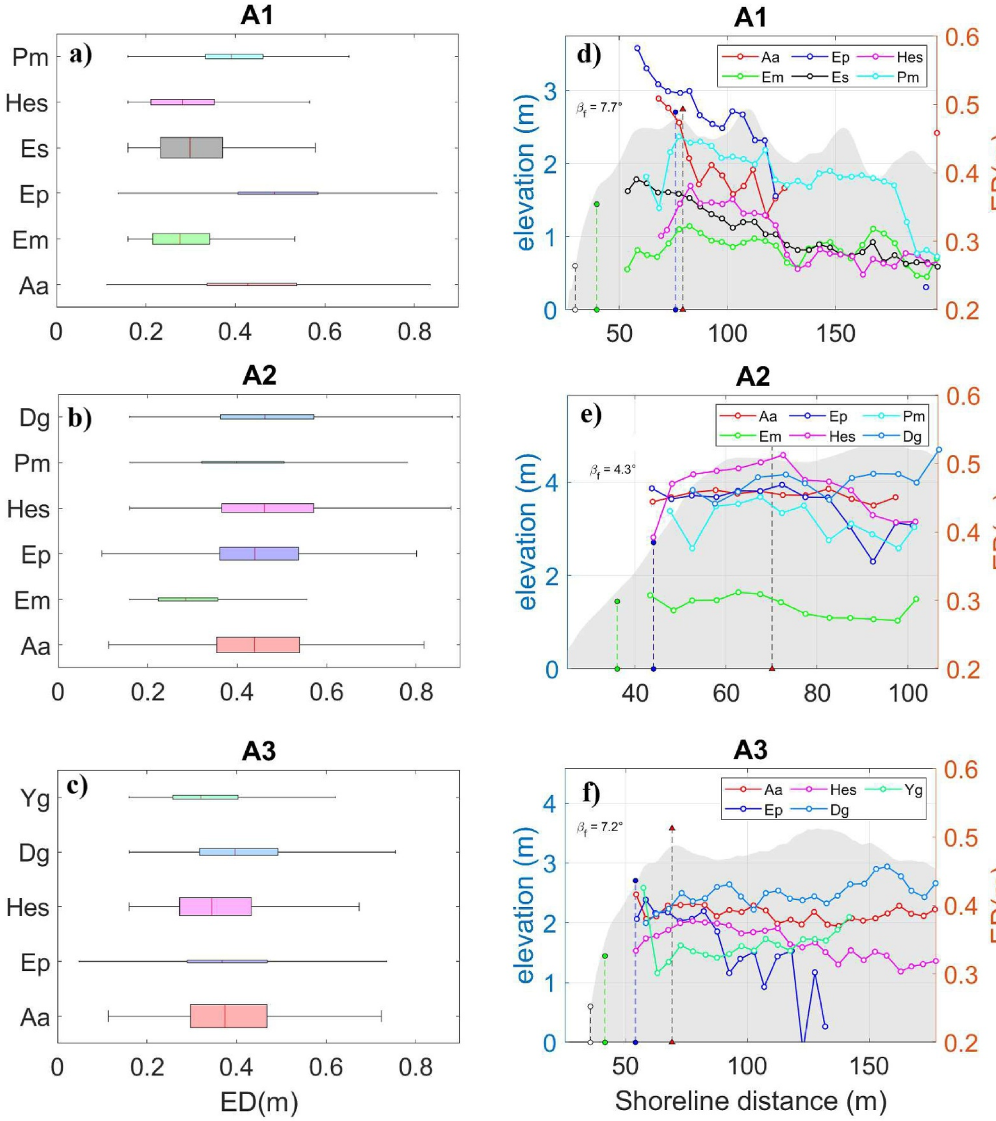

Figure 10. Boxplot of ED for every plant species in A1(a), A2(b) and A3(c). The width of the boxes is proportional to the abundance of the species in the study area. Distribution of mean Equivalent Diameter (ED) of each plant species along the direction perpendicular to the shoreline for A1 (d), A2 (e), and A3 (f). The mean topographic profile in this direction is highlighted in gray. The positions of the mean foredune crest (black dashed line with red triangles), mean total water level (blue dashed line with blue dots), 95th percentile (green dashed line with green dots), and 99th percentile (black dashed line with white dots) are also indicated. Abbreviations: *Aa*, (Ammophila arenaria); *Em*, (Eryngium maritimum); *Ep*, (Euphorbia paralias); *Es*, (Echinophora spinosa); *Hes*, (Helichrysum stoechas); *Pm*, (Pancratium maritimum); *Dg*, (Daphne gnidium); *Yg*, (Yucca gloriosa).

The decrease in vegetation density within the swash zone in A1 and A3 (Figures 11d–11f) is much more pronounced compared to the slight decrease of ED in the same region. Therefore, vegetation density appears to be more significantly impacted by runup than vegetation size. This may suggest that extreme wave events occur at intervals shorter than the time it takes for plants to reach maximum growth.

Vegetation size and density are crucial eco-morphological variables, reflecting the "health state" of plant species. We examined the relationship between these two by comparing the distance from the coastline of regions of maximum ED, denoting areas of greatest vegetation growth, and regions of minimum MND, indicating regions of highest vegetation density. Figure 12a illustrates that in A1, the maximum ED for all species occurs near the first

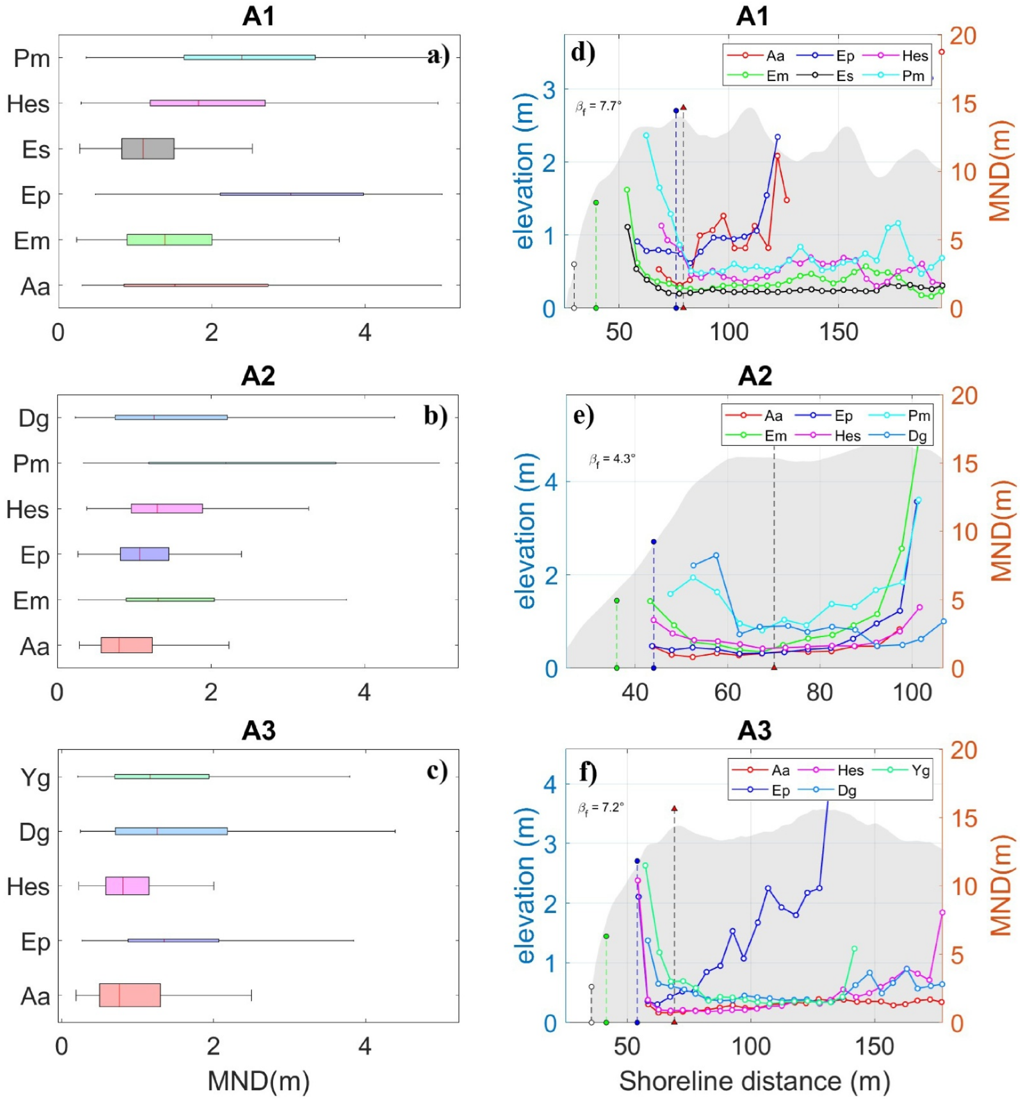

Figure 11. Boxplot of MND for every plant species in A1(a), A2(b) and A3(c). The width of the boxes is proportional to the abundance of the species in the study area. Distribution of MND of every plant species along the direction perpendicular to the shoreline for A1(d), A2(e) and A3(f). In gray, it's highlighted the mean topographic profile along the direction perpendicular to the shoreline. Are also highlighted the position of the mean foredune crest (black dashed line with red triangles), mean total water level(blue dashed line with blue dots), 95th percentile(green dashed line with green dots), 99th percentile(black dashed line with white dots). (Abbreviations: *Aa, Ammophila arenaria; Em, Eryngium maritimum; Ep, Euphorbia paralias; Es, Echinophora spinosa; Hes, Helichrysum stoechas; Pm, Pancratium maritimum; Dg, Daphne gnidium; Yg, Yucca gloriosa*).

crestline, as indicated by the abscissa of circles clustered around the A1 crestline's abscissa (marked with a small red dot). This suggests that in A1, areas of maximum ED are more closely associated with the crestline rather than regions of minimum MND, where higher vegetation growth is also expected. This is shown by the separation of circles from the bisector line in Figure 12a. Consequently, due to the uniform environmental conditions resulting from a flatter terrain morphology, the areas where plant species exhibit the most significant growth do not always align with the areas that provide optimal conditions for larger growth.

In A2 and A3, instead, the regions of maximum ED of all species show a correlation with regions of minimum MND, as we can see in Figure 12a, with square and diamond points clustering around the bisector line. Hence, in these cases, there exists a duality between the spatial density and plant size distribution for which regions of higher density correspond to regions of greatest growth. Furthermore, Figure 12b shows that all species have a

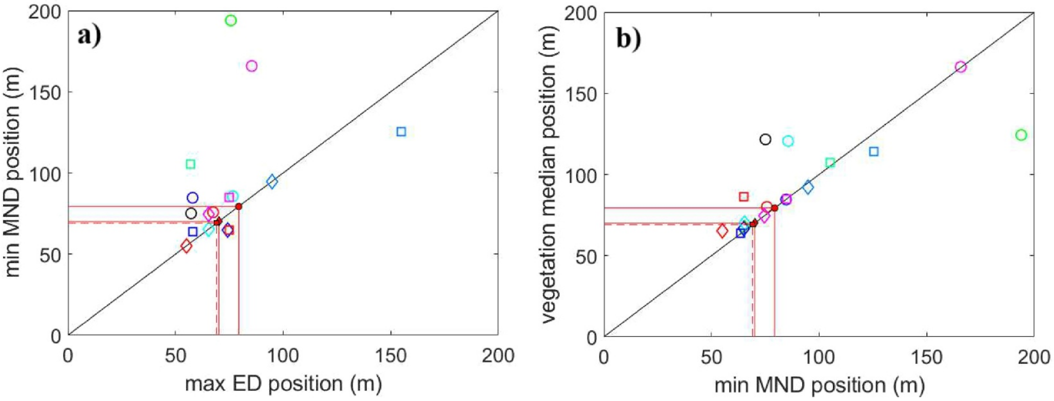

Figure 12. (a) Coordinate of maximum ED versus minimum MND in the across-shore direction; (b) Coordinate of minimum MND versus spatial distribution median in the across-shore direction. Circular, diamond and square dots represents data respectively from A1, A2 and A3. Each plant species is identified by a color: Red, Ammophila arenaria; green, Eryngium maritimum; blue, Euphorbia paralias; black, Echinophora spinosa; magenta, Helichrysum stoechas; cyan, Pancratium maritimum; sky blue, Daphne gnidium; water green, Yucca gloriosa. Are highlighted the positions of crestlines (red lines) and the bisector line (solid black line).

clear correlation between the regions of minimum MND and the position along the cross-shore direction of median of their spatial distribution (Figure 6), as denoted by diamond and square points aligning on the axis bisector.

3.5. Spatial Autocorrelation Analysis of Geometric Features

Experimental semivariograms and best-fitting models of ED and MND have been computed to analyze their spatial autocorrelation. The parameters of best-fitting theoretical semivariograms (i.e., *nugget*, range, *sill*), are summarized in Tables 3 and 4. The complete set of semivariograms are reported in the Figures S4–S9 of Supporting Information S1.

In nearly half of the cases, ED semivariograms show no discernible structure, with low R^2 values indicating a poor fit of theoretical models to the data. Consequently, these cases lack a noticeable spatial autocorrelation. Conversely, the remaining cases demonstrate well-defined semivariogram structures with high R^2 values, suggesting discernible spatial autocorrelation. However, despite clear structures, high nugget values (around 0.9) imply low autocorrelation even at distances shorter than the minimum lag distance (1 m in this study). This discrepancy may stem from either genuinely weak autocorrelation among neighboring plant sizes or noise in the data set due to segmentation inaccuracies in the OBIA algorithm, eventually necessitating the acquisition of ground truth data. Exceptions to this trend include *Helichrysum stoechas* and *Eryngium maritimum* in A1, which exhibit nugget values below 0.8, indicating slightly stronger spatial correlation.

Overall, the range of effective diameter (ED) remains within approximately 10 m, consistent with similar studies (Maestre et al., 2005), suggesting that vegetation diameter correlation diminishes over relatively short distances. This pattern may be attributed to the spatial cohesion of plants within individual patches of vegetation, which are correlated with neighboring plants but not with those outside their patch. Notably, *Ammophila arenaria* in A1 and A2 display wider ranges (33.7 and 66.0 m, respectively) compared to other species and even compared to the same species in A3 (range of 3.8 m).

Regarding the MND patterning, Table 4 reveals that over two-thirds of the cases have been excluded. These cases fail to align with any theoretical semivariogram model $\left(R^2 < 0.7\right)$. In contrast, the accepted cases exhibit MND semivariance nugget values significantly lower (ranging from 0.34 to 0.65) than those of EMD cases. This discrepancy suggests a notably less noisy data set and a stronger spatial autocorrelation at distances within the range. The quantity MND demonstrates a tendency to lose spatial autocorrelation over much greater distances compared to ED. Specifically, the range values fall between 17 and 36.7 m, with exception of *Helichrysum stoechas*, which displays a lower range of 4.02 m. This range is notably greater than the ED cases, where ranges

Table 3
Feature Parameters of ED Semi-Variograms, for Every Plant Species and Study Area

ED								
	Aa	Em	Ep	Es	Hes	Pm	Dg	Yg
Best Fit Model								
A1	gauss	exp	exp	exp	gauss	exp	–	–
A2	gauss	gauss	spherical	–	spherical	spherical	gauss	–
A3	exp	–	gauss	–	exp	–	spherical	spherical
R^2								
A1	0.75	0.99	0.37	0.91	0.89	0.87	–	–
A2	0.96	0.28	0.98	–	0.60	0.13	0.37	–
A3	0.93	–	0.71	–	0.77	–	0.49	0.38
Nugget(m)								
A1	0.87	0.7	0.82	0.8	0.73	0.8	–	–
A2	0.91	0.93	0.85	–	1.02	0.96	0.94	–
A3	0.93	–	0.96	–	0.89	–	0.98	0.97
Range(m)								
A1	33.7	10.7	63.5	3.5	6.11	45.9	–	–
A2	66.0	3.4	9.6	–	22.9	32.6	10.32	–
A3	3.8	–	–	–	2.0	–	39.2	18.2
Sill(m)								
A1	0.95	0.91	0.87	0.89	0.87	0.86	–	–
A2	0.96	0.98	1.03	–	1.04	1.02	0.99	–
A3	0.99	–	0.97	–	1.01	–	1.01	0.98

Note. Are highlighted in green the parameters of those semi-variograms satisfying the acceptance conditions described in paragraph 2.4.2.

span from 2 to 10.7 m (Table 3), excluding the outliers of 33.7 and 66 m for *Ammophila arenaria* in A1 and A2, as discussed previously.

3.6. Point Pattern Analysis

The results from the MNN analysis reveal a distinct clustered spatial arrangement among all species, as indicated by the r index being consistently less than 1 with high statistical significance, as Z-scores are below −1.96 (see Table 5). This clustering suggests that in environments with limited space, such as coastal dunes, short-range spatial variability in soil properties and environmental factors may play a more prominent role in determining vegetation patterns than competition for resources. This is because the environmental conditions in specific parts of the dune, such as soil composition, moisture levels, salinity, and microclimatic factors like temperature and wind exposure, create microhabitats that are favorable for certain species while being inhospitable to others (Kim & Yu, 2009). These localized differences result from the dynamic nature of coastal dune systems, where variations in elevation, proximity to the shoreline, and the influence of natural processes like sand deposition or erosion further shape the distribution of plant communities. As a result, species are often filtered by their ability to tolerate or thrive under the unique conditions of these microhabitats, leading to distinct vegetation patterns across the dune landscape. This aspect opens to mathematical modeling approaches, where the external stochastic forcing plays a relevant role. This is in contrast to ecosystems like forests, where the spatial variations of environmental conditions are less pronounced and resource competition is the main factor determining the spatial arrangement of vegetation, leading to more dispersed patterns (Szmyt & Stoyan, 2012).

It's worth noting that the same plant species in different study areas exhibit varying degrees of clustering, as lower r values indicating higher levels of clustering and more distinct patches, while higher r values, closer to 1, indicate

Table 4
Feature Parameters of MND Semi-Variograms, for Every Plant Species and Study Area

MND	Aa	Em	Ep	Es	Hes	Pm	Dg	Yg
Best Fit Model								
A1	gauss	gauss	spherical	gauss	exp	exp	–	–
A2	gauss	spherical	gauss	–	spherical	gauss	gauss	–
A3	gauss	–	exp	–	gauss	–	spherical	spherical
R^2								
A1	0.33	0.52	0.32	0.47	0.82	0.66	–	–
A2	0.49	0.69	0.96	–	0.41	0.36	0.35	–
A3	0.81	–	0.92	–	0.66	–	0.88	0.77
Nugget(m)								
A1	1.02	0.75	0.71	0.85	0.62	0.76	–	–
A2	0.69	0.57	0.47	–	1.07	1.19	1.13	–
A3	1.22	–	0.34	–	1.17	–	0.65	0.51
Range(m)								
A1	3.8	2.2	22.1	8.35	4.02	5.62	–	–
A2	5.4	20.9	27.19	–	5.2	32.2	36.28	–
A3	31.3	–	17	–	9.4	–	34.7	36.7
Sill(m)								
A1	1.35	0.82	1.06	1.05	0.97	0.98	–	–
A2	1.11	0.57	0.78	–	0.99	0.8	0.95	–
A3	0.9	–	1.17	–	0.96	–	1.03	1.13

Note. Are highlighted in green the parameters of those semi-variograms satisfying the acceptance conditions described in paragraph 2.4.2.

a more uncertain and "fuzzier" clustering pattern (P. Clark & Evans, 1954). An example is shown in Figure 13. Therefore, the degree of clustering cannot be considered as an attribute depending on the species of the plant.

In discussing the behavior of MND distribution in Section 3.4, we hypothesized a correlation between MND deviation (indicated by the inter-quartile range, IQR) and pattern type, noting that less abundant species tend to exhibit greater MND deviation, potentially leading to a more clustered pattern, and vice versa. The clustering degree, expressed by the nearest neighbor index *r*, can therefore be related to species abundance. To explore this relationship, the index *r* has been reported against abundance (Figure 14). The linear regression model shows an

Table 5
Nearest Neighbor Index, r, and Z-Score Values for Every Plant Species and Study Area

	Aa	Em	Ep	Es	Hes	Pm	Dg	Yg
r								
A1	0.35	0.7	0.46	0.72	0.65	0.65	–	–
A2	0.65	0.66	0.77	–	0.73	0.65	0.47	–
A3	0.63	–	0.49	–	0.64	–	0.47	0.43
Z-score								
A1	−43.3	−63.63	−30.67	−75.94	−52.75	−35.7	–	–
A2	−57.84	−37.41	−34.11	–	−32.37	−18.11	−43.61	–
A3	−101.87	–	−50.45	–	−93.95	–	−77.11	−76.96

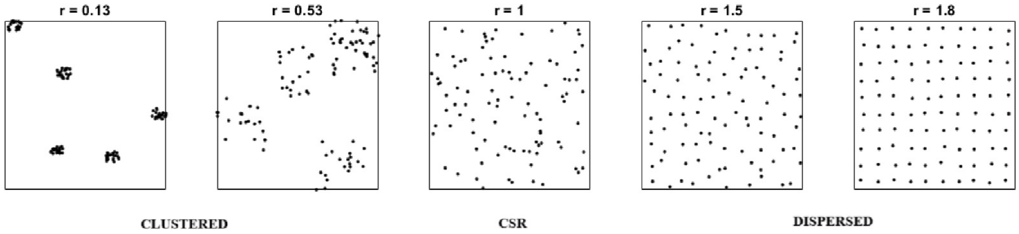

Figure 13. Example of five different synthetic spatial point patterns with their nearest neighbor index *r*. The lower the value of *r*, the higher the level of clustering or aggregation of points. The higher *r*, the higher the level of dispersion.

increase in *r* as a function of abundance, with a coefficient of determination $R^2 = 0.64$. While not ideal, this R^2 value is significant considering it reflects only abundance, without accounting for other potential error sources or the various factors influencing clustering, such as soil type, pH, and humidity.

Therefore, although the pattern type is always clustered for all cases ($r < 1$), less abundant species tend to exhibit higher levels of clustering compared to more abundant ones, coherently with the results of MND analysis.

The behavior of the modified Ripley's *L*-function confirms a statistically significant clustering pattern for all vegetation species, as $L(r)$ remains mostly in the top half of the graph, above the confidence interval (Figure 15). From Figure 15a, the *L*-function of *Ammophila arenaria* in A1 has 2 peaks at 22 and 50 m, indicating a clear clustering at 2 distinct spatial scales, as shown in the example in Figures 15d and 15e. Those two scales can be related to the topography of the study area, as they are multiples of the wavelength of the embryonic dunes in A1 which is about 25 m. Furthermore, at the largest scale of about 70 m, the pattern turns from clustered to dispersed, as the red $L(r)$ curve in Figure 15a drops below the confidence interval. The ground cover map of *Ammophila arenaria* shows clusters on the crest of the first two rows of dunes (Figure 15f). Other cases of multi-scale clusters can also be identified in those $L(d)$ curves that exhibit a plateau or multiple local maxima followed by a decrease. This could be the case of *Euphorbia paralias* in A1 (Figure 15a), with cluster scales ranging from about 30 to 50 m; *Daphne gnidium* in A2 (Figure 15b), with cluster scales from about 5 to 15 m; *Euphorbia paralias* in A3 (Figure 15c), with clusters scales from about 5 to 20 m.

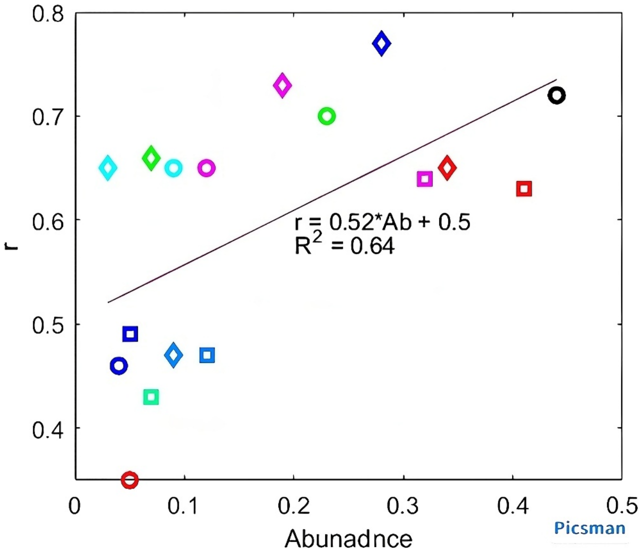

Figure 14. Abundance versus nearest neighbor index *r*. Linear regression of observed data is represented by the black solid line.

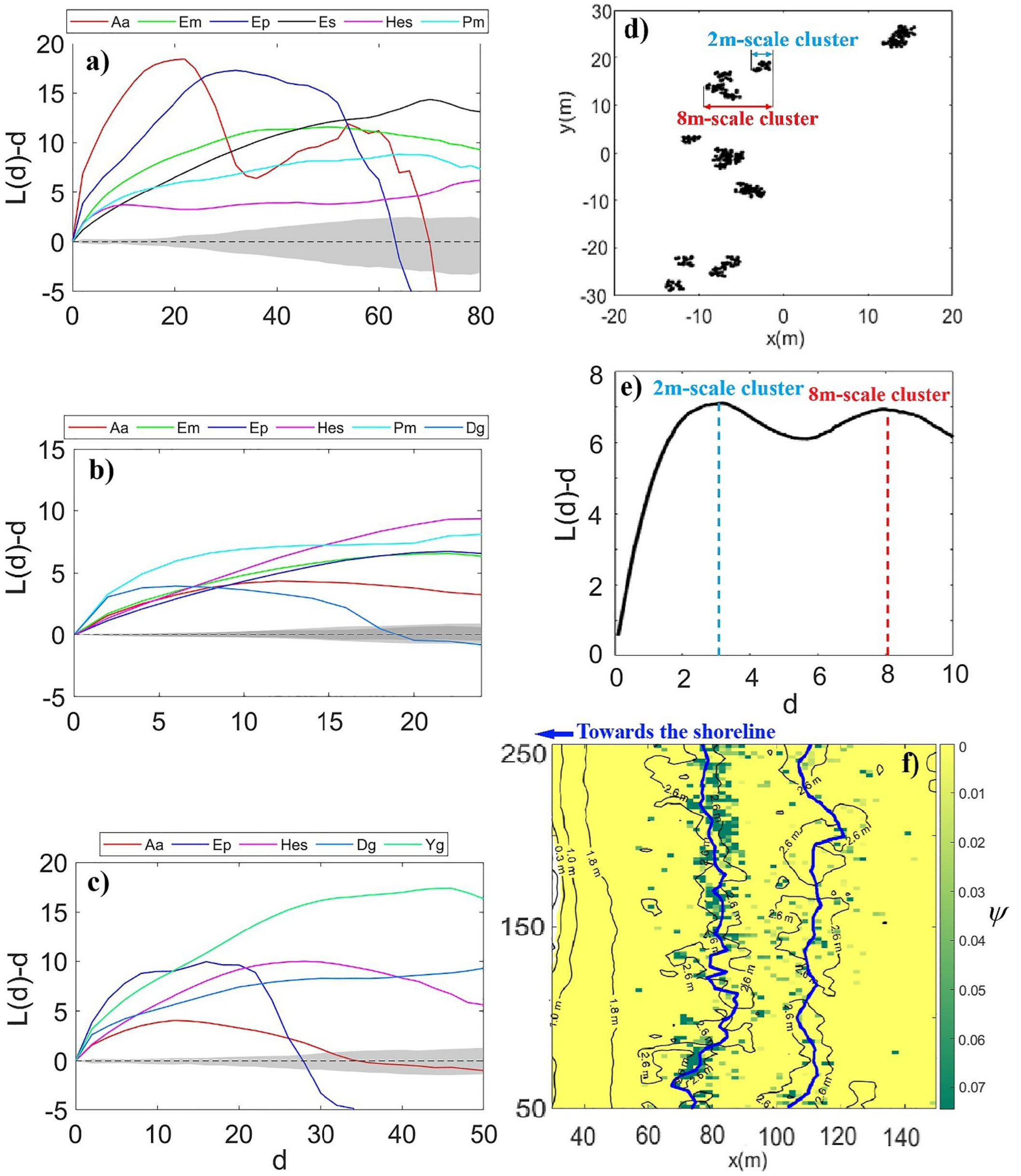

Figure 15. L-function for different plant species in A1(a), A2(b) and A3(c). The 95% confidence interval for the L-function computed through Monte Carlo simulation is highlighted in gray. (d) Example of a synthetic clustered spatial point pattern at two different scales: larger clusters at 8 m scale constituted by smaller clusters at 2 m scale. The two peaks in $L(d)$ graph (e) represent those two cluster scales and fall at distances d very close to 2 and 8 m. (f) Two-dimensional 2m-resolution Ground Cover map of *Ammophila arenaria* in A1. Contour lines of the elevation model (solid black lines) and crestline of the first and second row of shadow dunes (solid blue lines) are also plotted.

The pattern of *Euphorbia paralias* in A1 and A3 (Figures 15a–15c), shows a transition from a multi-scale cluster–even though with different sizes, probably due different extensions of study areas–to a dispersed pattern at largest scales, alike the case of *Ammophila arenaria* in A1. Other peculiar cases are the patterns of *Euphorbia paralias* in A2 (Figure 15b) and *Ammophila arenaria* in A3 (Figure 15c) which present a transition from clustered to random pattern as the scale increases, as $L(d)$ falls into the confidence interval, around 0. For all other cases, sizes of the main clusters are summarized in Table 6.

Table 6
Approximate Size of Plants Clusters Estimated With L-Function

	Cluster size(m)							
	Aa	Em	Ep	Es	Hes	Pm	Dg	Yg
A1	22	50	32	70	8	9	–	64
A2	12	22	22	–	26	27	6	–
A3	12	18	16	–	28	–	30	46

4. Conclusions

A large vegetation data set, derived by a machine learning classification algorithm, applied to ultra-high-resolution imagery of study areas, opens the possibility for a better insight into the complex inter-relationships between plant communities, terrain morphology, environmental forcings, and human presence, shaping sandy coastal dunes. Here we resume the key findings of the present research.

From the analysis of hydrodynamic forcings, we observed that, in well-formed dunefields, the threshold distance for vegetation growth is imposed by the reaching distance of wave runup during extreme events, acting as a cut-off for vegetation spatial distribution.

The morphology of the foredune is closely related to the abundance of dune-building species, like *Ammophila arenaria*, which also appears to be one of the most sensitive species to direct human disturbances. Abundance, in general, stands out as one of the main eco-morphological parameters in coastal vegetation pattern, as the dune morphology is commanded by the role of predominant species. Morphology, in turn, highly impacts the zonation: the higher the foredune, the more distinct the plant zonation; on the contrary, the flatter the terrain, the fuzzier and indistinct the zonation.

Interestingly, we found that the ratio of the vegetation threshold distance L_{veg} to the distance from the foredune crestline x_{crest} remains relatively consistent, independently from the terrain morphology. This aspect suggests further validation in other sites. Furthermore, in well-formed dunes systems, species exhibit consistent L_{veg}/x_{crest} ratios regardless of morphology. In all three study areas, among halophyte species, flooding appears to influence the L_{veg} only of *Ammophila arenaria*, highlighting the role of hydrodynamic forces on the spatial distribution of dune-building species and, consequently, on dune morphology.

Our analysis of Equivalent Diameter (ED) revealed that plant size statistical distribution is minimally affected by terrain morphology and abundance but is related to the species type. Instead, the spatial distribution of plant sizes is influenced by species abundance, with higher-abundance species exhibiting more uniform spatial distribution. In well-formed dune systems, there is a strong correlation between the distances from the coastline and the peaks of ED and Mean Neighbor Distance (MND). In contrast, on flatter and disturbed dunes, the peak ED is located around the first dune crestline, independent of the peak MND. Wave runup has a moderate detrimental effect on plant size, likely due to the frequency of extreme flooding events surpassing plant growth rates.

From the MND analysis, we observed that abundance strongly influences not only the mean plant density but also the pattern type of vegetation, with lower abundance species exhibiting a wider variation of local density, resulting in a clustering spatial pattern.

Semivariograms turned out not to be the best tool to analyze this type of data set for the high level of noise in the data set. Noise emerges when there are errors in measures and, in this case, the measure of ED and MND heavily depends on the accuracy of the classification algorithm. Despite the challenges posed by noise in the data set, semivariograms highlighted the limited spatial autocorrelation of plant size and the larger-scale autocorrelation of plant density.

The Mean Nearest Neighbor point pattern analysis revealed a clustered spatial arrangement for all species taken into exam, although, the degree of clustering is correlated with the abundance, confirming that abundance is the main factor controlling the pattern type of a plant species: Notably, the L-function emerged as a valuable tool for elucidating the type and scales of vegetation clusters, revealing multi-scale clustering patterns for many coastal species.

With this work, we aim to provide a species-by-species extensive qualitative and quantitative description of vegetation spatial patterns using different geostatistical tools, widely used in spatial analysis and vegetation studies.

In conclusion, we believe that the methods proposed for studying vegetation patterns offer valuable insights into the complex interplay between biotic and abiotic processes occurring in coastal dunes, thereby enhancing environmental monitoring and conservation efforts. Additionally, the patterns identified in this study can serve as a foundation for fine-tuning and validating numerical eco-morphodynamic models in these study sites, further advancing our understanding of these dynamic ecosystems.

Conflict of Interest

The authors declare no conflicts of interest relevant to this study.

Data Availability Statement

All the MATLAB codes and data used for this paper (Demichele et al., 2025), including DTMs, ortho-images, vegetation data and wave data are available at: https://doi.org/10.5281/zenodo.13220981.

Acknowledgments
This work is supported by the Ente Parco Regionale Migliarino San Rossore Massaciuccoli, which granted access to the park's restricted areas and authorized field activities. We also thank Paolo Maschio for conducting the UAV surveys and Andrea Cagninei, Luca Salerno, Melissa Latella, and Elisa Caccamo for their support to the field measurements. Open access publishing facilitated by Politecnico di Torino, as part of the Wiley - CRUI-CARE agreement.

References

Acosta, A., Carranza, M. L., & Izzi, C. (2005). Combining land cover mapping of coastal dunes with vegetation analysis. *Applied Vegetation Science*, *8*(2), 133–138. https://doi.org/10.1658/1402-2001(2005)008[0133:clcmoc]2.0.co;2

Acosta, A., & Ercole, S. (2015). *Gli habitat delle coste sabbiose italiane: ecologia e problematiche di conservazione*. Ispra. serie rapporti, 215/2015.

Ahmad, A. M., Minallah, N., Ahmed, N., Ahmad, A. M., & Fazal, N. (2020). Remote sensing based vegetation classification using machine learning algorithms. In *2019 international conference on Advances in the Emerging Computing Technologies (AECT)* (pp. 1–6).

Alquini, F., Bertoni, D., & Sarti, G. (2016). Extreme erosion of a dune crest within a short timespan (January–September 2016): The recent case in the migliarino–san rossore–massaciuccoli regional park (Tuscany, Italy). Atti Della Società Toscana di Scienze Naturali (Pisa). *Memorie. Serie A*, *123*, 5–11.

Barducci, A., Guzzi, D., Marcoionni, P., & Pippi, I. (2009). Aerospace wetland monitoring by hyperspectral imaging sensors: A case study in the coastal zone of san Rossore Natural park. *Journal of Environmental Management*, *90*(7), 2278–2286. https://doi.org/10.1016/j.jenvman.2007.06.033

Belcore, E., Latella, M., Piras, M., & Camporeale, C. (2024). Enhancing precision in coastal dunes vegetation mapping: Ultra-high resolution hierarchical classification at the individual plant level. *International Journal of Remote Sensing*, *45*(13), 4527–4552. https://doi.org/10.1080/01431161.2024.2354135

Belcore, E., Pittarello, M., Lingua, A. M., & Lonati, M. (2021). Mapping riparian habitats of Natura 2000 network (91e0*, 3240) at individual tree level using UAV multi-temporal and multi-spectral data. *Remote Sensing*, *13*(9), 1756. https://doi.org/10.3390/rs13091756

Berhane, T. M., Lane, C. R., Wu, Q., Anenkhonov, O. A., Chepinoga, V. V., Autrey, B. C., & Liu, H. (2017). Comparing pixel-and object-based approaches in effectively classifying wetland-dominated landscapes. *Remote Sensing*, *10*(1), 46. https://doi.org/10.3390/rs10010046

Bermúdez, R., & Retuerto, R. (2013). Living the difference: Alternative functional designs in five perennial herbs coexisting in a coastal dune environment. *Functional Plant Biology*, *40*(11), 1187–1198. https://doi.org/10.1071/fp12392

Bertacchi, A. (2017). Dune habitats of the migliarino–san rossore–massaciuccoli regional park (Tuscany–Italy). *Journal of Maps*, *13*(2), 322–331. https://doi.org/10.1080/17445647.2017.1302365

Bertacchi, A., Zuffi, M. A. L., & Lombardi, T. (2016). Foredune psammophilous communities and coastal erosion in a stretch of the Ligurian sea (Tuscany, Italy). *Rendiconti Lincei*, *27*(4), 639–651. https://doi.org/10.1007/s12210-016-0543-5

Besag, J., & Diggle, P. J. (1977). Simple Monte Carlo tests for spatial pattern. *Journal of the Royal Statistical Society—Series C: Applied Statistics*, *26*(3), 327–333. https://doi.org/10.2307/2346974

Bressolier, C., & Thomas, Y.-F. (1977). Studies on wind and plant interactions on French Atlantic coastal dunes. *Journal of Sedimentary Research*, *47*(1), 331–338.

Carter, R., & Wilson, P. (1993). Aeolian processes and deposits in northwest Ireland. *Geological Society, London, Special Publications*, *72*(1), 173–190. https://doi.org/10.1144/gsl.sp.1993.072.01.15

Chu, D., & Chu, D. (2020). Fractional vegetation cover. In *Remote sensing of land use and land cover in mountain region: A comprehensive study at the central Tibetan plateau* (pp. 195–207).

Ciccarelli, D., Cini, E., Mo, A., Paterni, M., Massetti, L., Rangel-Buitrago, N., & Merlino, S. (2023). The assessment and management of plant invasions with unmanned aerial vehicles. The yucca Gloriosa case, Italy. *Regional Studies in Marine Science*, *57*, 102759. https://doi.org/10.1016/j.rsma.2022.102759

Cipriani, L. E., Perfetti, A., Pranzini, E., & Vitale, G. (2010). Azioni di Tutela Delle dune costiere del parco regionale migliarino san rossore massaciuccoli (Toscana Settentrionale). *Studi costieri*, *17*, 165–179.

Clark, J. (1977). *Coastal ecosystems management: A technical manual for the conservation of coastalzone resources* (p. 928). Wiley-Interscience.

Clark, P., & Evans, F. (1954). Distance to nearest neighbor as a measure of spatial relationships in populations. *Ecology*, *35*(4), 445–453. https://doi.org/10.2307/1931034

Coulloudon, B., Eshelman, K., Gianola, J., Habich, N., Hughes, L., Johnson, C., et al. (1999). Sampling vegetation attributes: Interagency technical reference.

Curr, R., Koh, A., Edwards, E., Williams, A., & Davies, P. (2000). Assessing anthropogenic impact on mediterranean sand dunes from aerial digital photography. *Journal of Coastal Conservation*, *6*(1), 15–22. https://doi.org/10.1007/bf02730463

Darke, P. R., Brady, M. K., Benedicktus, R. L., & Wilson, A. E. (2016). Feeling close from Afar: The role of psychological distance in offsetting distrust in unfamiliar online retailers. *Journal of Retailing*, *92*(3), 287–299. https://doi.org/10.1016/j.jretai.2016.02.001

Demichele, D., Belcore, E., Piras, M., & Camporeale, C. (2025). Species-by-species pattern analysis of coastal dune vegetation [Dataset]. *Zenodo*. https://doi.org/10.5281/zenodo.13220981

Dixon, P. M. (2002). Nearest-neighbor contingency table analysis of spatial segregation for several species. *Écoscience*, *9*(2), 142–151. https://doi.org/10.1080/11956860.2002.11682700

Durán, O., & Moore, L. J. (2013). Vegetation controls on the maximum size of coastal dunes. *Proceedings of the National Academy of Sciences*, *110*(43), 17217–17222. https://doi.org/10.1073/pnas.1307580110

Eamer, J. B., Darke, I. B., & Walker, I. J. (2013). Geomorphic and sediment volume responses of a coastal dune complex following invasive vegetation removal. *Earth Surface Processes and Landforms*, *38*(10), 1148–1159. https://doi.org/10.1002/esp.3403

Frederiksen, L., Kollmann, J., Vestergaard, P., & Bruun, H. H. (2006). A multivariate approach to plant community distribution in the coastal dune zonation of NW Denmark. *Phytocoenologia*, *36*(3), 321–342. https://doi.org/10.1127/0340-269x/2006/0036-0321

French, K. (2012). Competition strength of two significant invasive species in coastal dunes. *Plant Ecology*, *213*(10), 1667–1673. https://doi.org/10.1007/s11258-012-0122-5

Gadgil, R. (2002). Marram grass (Ammophila Arenaria) and coastal sand stability in New Zealand. *New Zealand Journal of Forestry Science*, *32*(2), 165–180.

Gellini, R., Pantani, F., Grossoni, P., Bussotti, F., Barbolani, E., & Rinallo, C. (1983). Survey of the deterioration of the coastal vegetation in the park of san rossore in central Italy. *European Journal of Forest Pathology*, *13*(5–6), 296–304. https://doi.org/10.1111/j.1439-0329.1983.tb00130.x

Goreaud, F., & Pélissier, R. (1999). On explicit formulas of edge effect correction for Ripley's k-function. *Journal of Vegetation Science*, *10*(3), 433–438. https://doi.org/10.2307/3237072

Grootjans, A., Geelen, H., Jansen, A., & Lammerts, E. (2002). Restoration of coastal dune slacks in The Netherlands. *Ecological restoration of aquatic and semi-aquatic ecosystems in the Netherlands (NW Europe)*, 181–203. https://doi.org/10.1007/978-94-017-1335-1_10

Haase, P. (1995). Spatial pattern analysis in ecology based on Ripley's k-function: Introduction and methods of edge correction. *Journal of Vegetation Science*, *6*(4), 575–582. https://doi.org/10.2307/3236356

Hertling, U., & Lubke, R. (1999). Use of Ammophila Arenaria for dune stabilization in South Africa and its current distribution—Perceptions and problems. *Environmental Management*, *24*(4), 467–482. https://doi.org/10.1007/s002679900247

Hesp, P. (1988). Morphology, dynamics and internal stratification of some established Foredunes in southeast Australia. *Sedimentary Geology*, *55*(1–2), 17–41. https://doi.org/10.1016/0037-0738(88)90088-7

Hesp, P. (1991). Ecological processes and plant adaptations on coastal dunes. *Journal of Arid Environments*, *21*(2), 165–191. https://doi.org/10.1016/s0140-1963(18)30681-5

Hesp, P. (2002). Foredunes and blowouts: Initiation, geomorphology and dynamics. *Geomorphology*, *48*(1–3), 245–268. https://doi.org/10.1016/s0169-555x(02)00184-8

Hewett, D. (1970). The colonization of sand dunes after stabilization with marram grass (ammophila arenaria). *Journal of Ecology*, *58*(3), 653–668. https://doi.org/10.2307/2258527

Hunt, I. A., Jr. (1959). Design of seawalls and breakwaters. *Journal of the Waterways and Harbors Division*, *85*(3), 123–152. https://doi.org/10.1061/jwheau.0000129

Joshi, N., Suresh, H., Dattaraja, H., & Sukumar, R. (1997). The spatial organization of plant communities in a deciduous forest: A computational-geometry-based analysis. *Journal of the Indian Institute of Science*, *77*(4), 365.

Kattenborn, T., Leitloff, J., Schiefer, F., & Hinz, S. (2021). Review on Convolutional Neural Networks (CNN) in vegetation remote sensing. *ISPRS Journal of Photogrammetry and Remote Sensing*, *173*, 24–49. https://doi.org/10.1016/j.isprsjprs.2020.12.010

Kim, D., & Yu, K. B. (2009). A conceptual model of coastal dune ecology synthesizing spatial gradients of vegetation, soil, and geomorphology. *Plant Ecology*, *202*(1), 135–148. https://doi.org/10.1007/s11258-008-9456-4

Kiskowski, M. A., Hancock, J. F., & Kenworthy, A. K. (2009). On the use of Ripley's k-function and its derivatives to analyze domain size. *Biophysical Journal*, *97*(4), 1095–1103. https://doi.org/10.1016/j.bpj.2009.05.039

Kowe, P., Mutanga, O., Odindi, J., & Dube, T. (2019). Exploring the spatial patterns of vegetation fragmentation using local spatial autocorrelation indices. *Journal of Applied Remote Sensing*, *13*(2), 024523. https://doi.org/10.1117/1.jrs.13.024523

Lee, S., Wolberg, G., & Shin, S. Y. (1997). Scattered data interpolation with multilevel b-splines. *IEEE Transactions on Visualization and Computer Graphics*, *3*(3), 228–244. https://doi.org/10.1109/2945.620490

Leucci, G., De Giorgi, L., & Scardozzi, G. (2014). Geophysical prospecting and remote sensing for the study of the san Rossore area in Pisa (Tuscany, Italy). *Journal of Archaeological Science*, *52*, 256–276. https://doi.org/10.1016/j.jas.2014.08.028

Lo, C., & Quattrochi, D. A. (2003). Land-use and land-cover change, urban heat island phenomenon, and health implications. *Photogrammetric Engineering and Remote Sensing*, *69*(9), 1053–1063. https://doi.org/10.14358/pers.69.9.1053

Maestre, F. T., Rodríguez, F., Bautista, S., Cortina, J., & Bellot, J. (2005). Spatial associations and patterns of perennial vegetation INA semi-arid steppe: A multivariate geostatistics approach. *Plant Ecology*, *179*(2), 133–147. https://doi.org/10.1007/s11258-004-4641-6

Martínez, M. L., Hesp, P. A., & Gallego-Fernández, J. B. (2013). Coastal dunes: Human impact and need for restoration. *Restoration of coastal dunes*, 1–14. https://doi.org/10.1007/978-3-642-33445-0_1

Martínez, M. L., & Psuty, N. P. (2004). *Coastal dunes*. Springer.

Martínez Prentice, R., Villoslada Peciña, M., Ward, R. D., Bergamo, T. F., Joyce, C. B., & Sepp, K. (2021). Machine learning classification and accuracy assessment from high-resolution images of coastal wetlands. *Remote Sensing*, *13*(18), 3669. https://doi.org/10.3390/rs13183669

Matheron, G. (1963). Principles of geostatistics. *Economic Geology*, *58*(8), 1246–1266. https://doi.org/10.2113/gsecongeo.58.8.1246

Maximiliano-Cordova, C., Martínez, M. L., Silva, R., Hesp, P. A., Guevara, R., & Landgrave, R. (2021). Assessing the impact of a winter storm on the beach and dune systems and erosion mitigation by plants. *Frontiers in Marine Science*, *8*, 734036. https://doi.org/10.3389/fmars.2021.734036

Michez, A., Piégay, H., Lisein, J., Claessens, H., & Lejeune, P. (2016). Classification of riparian forest species and health condition using multi-temporal and hyperspatial imagery from unmanned aerial system. *Environmental Monitoring and Assessment*, *188*(3), 1–19. https://doi.org/10.1007/s10661-015-4996-2

Morrison, L. W. (2016). Observer error in vegetation surveys: A review. *Journal of Plant Ecology*, *9*(4), 367–379. https://doi.org/10.1093/jpe/rtv077

Muñoz-Reinoso, J. C. (2018). Doñana mobile dunes: What is the vegetation pattern telling us? *Journal of Coastal Conservation*, *22*(4), 605–614. https://doi.org/10.1007/s11852-018-0594-0

Myllymäki, M., Mrkvička, T., Grabarnik, P., Seijo, H., & Hahn, U. (2017). Global envelope tests for spatial processes. *Journal of the Royal Statistical Society—Series B: Statistical Methodology*, *79*(2), 381–404. https://doi.org/10.1111/rssb.12172

Nay, J., Burchfield, E., & Gilligan, J. (2018). A machine-learning approach to forecasting remotely sensed vegetation health. *International Journal of Remote Sensing*, *39*(6), 1800–1816. https://doi.org/10.1080/01431161.2017.1410296

Nehren, U., Thai, H. H. D., Marfai, M. A., Raedig, C., Alfonso, S., Sartohadi, J., & Castro, C. (2016). Ecosystem services of coastal dune systems for hazard mitigation: Case studies from Vietnam, Indonesia, and Chile. In *Ecosystem-based disaster risk reduction and adaptation in practice* (pp. 401–433).

Oosting, H. J. (1945). Tolerance to salt Spary of plants of coastal dunes. *Ecology*, *26*(1), 85–89. https://doi.org/10.2307/1931917

Pélissier, R., & Goreaud, F. (2001). A practical approach to the study of spatial structure in simple cases of heterogeneous vegetation. *Journal of Vegetation Science*, *12*(1), 99–108. https://doi.org/10.1111/j.1654-1103.2001.tb02621.x

Pranzini, E. (2018). Shore protection in Italy: From hard to soft engineering. and back. *Ocean and Coastal Management*, *156*, 43–57. https://doi.org/10.1016/j.ocecoaman.2017.04.018

Ripley, B. (1984). *198 1. Spatial statistics*. Wiley and Sons.

Sadahiro, Y. (2024). Event pattern analysis: Peak detection and pattern comparison. *Geographical Analysis*, *56*(1), 143–162. https://doi.org/10.1111/gean.12372

Schandry, N., & Becker, C. (2020). Allelopathic plants: Models for studying plant–interkingdom interactions. *Trends in Plant Science*, *25*(2), 176–185. https://doi.org/10.1016/j.tplants.2019.11.004

Scopetani, C., Chelazzi, D., Martellini, T., Pellinen, J., Ugolini, A., Sarti, C., & Cincinelli, A. (2021). Occurrence and characterization of microplastic and mesoplastic pollution in the migliarino san rossore, massaciuccoli nature park (Italy). *Marine Pollution Bulletin*, *171*, 112712. https://doi.org/10.1016/j.marpolbul.2021.112712

Shi, Y., Wang, T., Skidmore, A. K., & Heurich, M. (2020). Improving Lidar-based tree species mapping in central European mixed forests using multi-temporal digital aerial colour-infrared photographs. *International Journal of Applied Earth Observation and Geoinformation*, *84*, 101970. https://doi.org/10.1016/j.jag.2019.101970

Short, A. D., & Hesp, P. A. (1982). Wave, beach and dune interactions in Southeastern Australia. *Marine Geology*, *48*(3–4), 259–284. https://doi.org/10.1016/0025-3227(82)90100-1

Sigren, J. M., Figlus, J., & Armitage, A. R. (2014). Coastal sand dunes and dune vegetation: Restoration, erosion, and storm protection. *Shore and Beach*, *82*(4), 5–12.

Silva, R., Martínez, M., Odériz, I., Mendoza, E., & Feagin, R. (2016). Response of vegetated dune–beach systems to storm conditions. *Coastal Engineering*, *109*, 53–62. https://doi.org/10.1016/j.coastaleng.2015.12.007

Silvestri, S., Marani, M., & Marani, A. (2003). Hyperspectral remote sensing of salt marsh vegetation, morphology and soil topography. *Physics and Chemistry of the Earth, Parts A/B/C*, *28*(1–3), 15–25. https://doi.org/10.1016/s1474-7065(03)00004-4

Stockdon, H., Holman, R., Howd, P., Sallenger, J., & Asbury, H. (2006). Empirical parameterization of setup, swash, and Runup. *Coastal Engineering*, *53*(7), 573–588. https://doi.org/10.1016/j.coastaleng.2005.12.005

Sykes, M. T., & Wilson, J. B. (1988). An experimental investigation into the response of some New Zealand sand dune species to salt spray. *Annals of Botany*, *62*(2), 159–166. https://doi.org/10.1093/oxfordjournals.aob.a087646

Szmyt, J., & Stoyan, D. (2012). Spatial structure of managed beech-dominated forest: Applicability of nearest neighbors indices. *Dendrobiology*, *68*, 129–136. https://doi.org/10.12657/denbio.071.013

Tucker, C. J. (1979). Red and photographic infrared linear combinations for monitoring vegetation. *Remote Sensing of Environment*, *8*(2), 127–150. https://doi.org/10.1016/0034-4257(79)90013-0

Vosselman, G. (2000). Slope based filtering of laser altimetry data. *International archives of photogrammetry and remote sensing*, *33*(B3/2; PART 3), 935–942.

Walker, I. J., Eamer, J. B., & Darke, I. B. (2013). Assessing significant geomorphic changes and effectiveness of dynamic restoration in a coastal dune ecosystem. *Geomorphology*, *199*, 192–204. https://doi.org/10.1016/j.geomorph.2013.04.023

Whiteside, T. G., Boggs, G. S., & Maier, S. W. (2011). Comparing object-based and pixel-based classifications for mapping Savannas. *International Journal of Applied Earth Observation and Geoinformation*, *13*(6), 884–893. https://doi.org/10.1016/j.jag.2011.06.008

Xie, Y., Sha, Z., & Yu, M. (2008). Remote sensing imagery in vegetation mapping: A review. *Journal of Plant Ecology*, *1*(1), 9–23. https://doi.org/10.1093/jpe/rtm005

Yousefi Lalimi, F., Silvestri, S., Moore, L., & Marani, M. (2017). Coupled topographic and vegetation patterns in coastal dunes: Remote sensing observations and ecomorphodynamic implications. *Journal of Geophysical Research: Biogeosciences*, *122*(1), 119–130. https://doi.org/10.1002/2016jg003540